CONTROLLED FABRICATION SYSTEM OF FABRY-PEROT OPTICAL FIBER SENSORS

by

Wei Huo

Thesis submitted to the faculty of the
Virginia Polytechnic Institute and State University
in partial fulfillment of the requirements for the degree of

MASTER OF SCIENCE

in

Electrical Engineering

APPROVED BY:

Anbo Wang, Chairman

Russell May

Brian D. Woerner

July 10th, 2000
Blacksburg, Virginia

Keywords: Optical Fiber, White Light Interferometer, CO_2 Laser Control, PZT, Real-time Control

Controlled Fabrication System of Fabry-Perot Optical Fiber Sensors

by

Wei Huo

Anbo Wang, Chairman

The Bradley Department of Electrical and Computer Engineering, Virginia Tech

(Abstract)

The use of optical fiber sensors is increasing widely in industry, civil, medicine, defense and research. Among different categories of these sensors is the Extrinsic Fabry-Perot interferometer (EFPI) sensor which is inherently simple and requires only modest amount of interface electronics. These advantages make it suitable for many practical applications. Investigating a cost-effective, reliable and repeatable method for optical fiber sensor fabrication is challenging work. In this thesis, a system for controlled fabrication of Fabry-Perot optical fiber sensors is developed and presented as the first attempt for the long-term goal of automated EFPI sensor fabrication. The sensor fabrication control system presented here implements a real-time control of a carbon dioxide (CO_2) laser as sensor bonding power, an optical fiber white light interferometric subsystem for real-time monitoring and measurement of the air gap separation in the Fabry-Perot sensor probe, and real-time control of a piezoelectric (PZT) motion subsystem for sensor alignment. The design of optoelectronic hardware and computer software is included. A large number of sensors are fabricated using this system and are tested under high temperature and high pressure. This system as a prototype system shows the potential in automated sensor fabrication.

Acknowledgements

First and foremost, I would like to thank Dr. Anbo Wang, my advisor and graduate committee chair, for his thoughtful guidance and constant encouragement and for giving me the opportunity to work at Photonics Lab as his graduate student. I am extremely grateful to Dr. Russell May for his valuable help from time to time. My thanks also go to Dr. Brian Woerner as a member of my committee who is one of my favorite professors. Special thanks to Hai Xiao, who directly supervised the progress and designed the mechanical part of the sensor supporting system. I am grateful to Ming Luo, who did the design of the DAC, Zhiyong Wang, who did electric circuits for single mode and multimode systems, Bing Qi and Jiangdong Deng, who gave me great suggestions during my research work. I express my gratitude to all the people at Photonics Lab who made it an enjoyable place and filled my time there with unforgettable memories.

Last but not least, I am thankful to my parents and all my brothers and sisters for providing me support. I am very thankful to my husband and my daughter, who have always wished the best for me and showered all their love and affection on me.

* The presented sensor fabrication control system research is part of an ongoing 4-year project on Optical Fiber Sensor Technologies for the Efficient and Economical Oil Recovery program at Photonics Lab, Virginia Tech, jointly funded by the Federal Energy Technology Center of the U.S. Department of Energy (DOE) and Chevron.

Table of Contents

List of Figures

Chapter 1. Introduction

1.1 Fiber-based Optical Sensors

Optical fiber sensors have established themselves in sensor instrumentation during the past two decades. They have certain advantages over many conventional sensors in their immunity to electromagnetic interference (EMI), achievable ultra-high sensitivity, basic low cost components, small size, environmental ruggedness to vibration and shock, and last but not least, their large bandwidths to offer their distinct advantages in their ability to transport the resultant data [1].

Because of these advantages, the widespread development and widening applications of optical fiber sensors are increasing in industry [2], civil engineering [3,4,5], medicine [6], and defense. Some of these applications include gyroscopes for automotive navigation systems [7], strain sensors for smart structures [8], and a variety of fiber optic sensors for the measurement of physical and electrical parameters such as temperature, pressure, fluid flow, acoustics, acceleration, voltage and current in process control applications.

Fiber sensors are classified according to the transduction mechanism which brings about a change in some property of optical waves propagating in the fiber, such as intensity, phase, polarization, modal content, etc. Hence the corresponding sensors are known as intensity-based, phase- or interferometeric-based, polarimetric-type, and modal content-based.

Interferometeric sensors offer the advantages of geometric versatility of the sensing element, wide dynamic range, and extremely high sensitivity [1]. Interferometeric sensors are classified by their geometry as being Fabry-Perot, Mach-Zehnder, Michelson, and Sagnac [1]. All the interferometric sensors have maximum sensitivity at the quadrature (Q) point. So the signal must be maintained at the Q point in order to avoid loss of sensitivity. To overcome this limitation, some methods have been proposed and developed, such as quadrature phase shifted operation, dual wavelength method, and white light interferometry. White light interferometric systems have several inherent advantages, though their signal processing

techniques are more complex. Among the advantages are high precision, excellent resolution, the self-calibrating capabilities, and the wide unambiguous dynamic range of operation [9].

Fiber sensors are also classified as being extrinsic and intrinsic, referring to the sensing region of the fiber sensor being outside or inside the fiber, respectively. In intrinsic sensors, the optical waves in the fiber are affected directly by the incident perturbation, and changes in the output intensity give an indication of the magnitude of the disturbance. One such an example is the intrinsic Fabry-Perot interferometeric sensor (IFPI) [10,11]. The IFPI system consists of a monochromatic source such as a laser diode that injects light into one of the input arms of a 2x2 bidirectional single-mode coupler. The Fabry-Perot cavity is formed by placing a segment of a single mode fiber that has both endfaces coated with a semi-transparent reflective coating on one of the output arms of the coupler. The signals that form the interference pattern are reflected from the two ends of this fused fiber segment. Yet in extrinsic sensors, the fiber only serves to carry optical power to, and the sensing information from, an external region. The resonant cavity of an extrinsic Fabry-Perot interferometer (EFPI) is formed by placing two optical fibers in an alignment tube separated by an air gap. Extrinsic Fabry-Perot interferometeric (EFPI) sensors have been implemented for the measurement of strain [12], temperature [13], and vibration mode analysis in smart structures [14].

Today, the field of measurement and instrumentation, and in particular of sensor development has expanded rapidly. With the approach of the 21st century, the need for high quality sensors to be integrated into sophisticated measurement and control systems is clear. In parallel with the rapid advance in the development of sensors, a cost-effective, reliable and repeatable sensor fabrication technology becomes more significant.

1.2 EFPI Optic Fiber Sensor Fabrication

Fiber Fabry-Perot sensors have been used for many years. They are highly sensitive to temperature, mechanical vibration, magnetic fields, and acoustic waves. Although Intrinsic Fabry-Perot sensors have been used in the past to measure several parameters, extrinsic Fabry-Perot (EFPI) sensors have shown their ability to be immune to lightwave polarization and only sensitive to axial strain components. By examining the interferometric output

spectrum of an EFPI sensor, we can determine the absolute air gap cavity length without initialization [15, 16]. It is possible to design the interferometer to only sense one or two parameters which eliminate response to interfering parameters. This allows construction of, for example, pressure sensors that are not temperature sensitive [1].

Various fiber sensors have been realized by different methods and have shown very good capabilities. The main drawback, however, is lack of mass fabrication methods allowing good reproducibility and a minimized number of processing steps. To date most of the EFPI fiber sensors are fabricated manually, and the tube and fibers are glued with epoxies [13,17]. The performance of a sensor fabricated by this method is very dependent on the characteristics of the epoxy. As a result, this method is lack of not only fabrication repeatability but also air gap control. Although some people fabricated sensors using thermal bonding recently [16], they used a torch as the heating source. It is very difficult to control accurately the power of the torch and the air gap separation of the sensor.

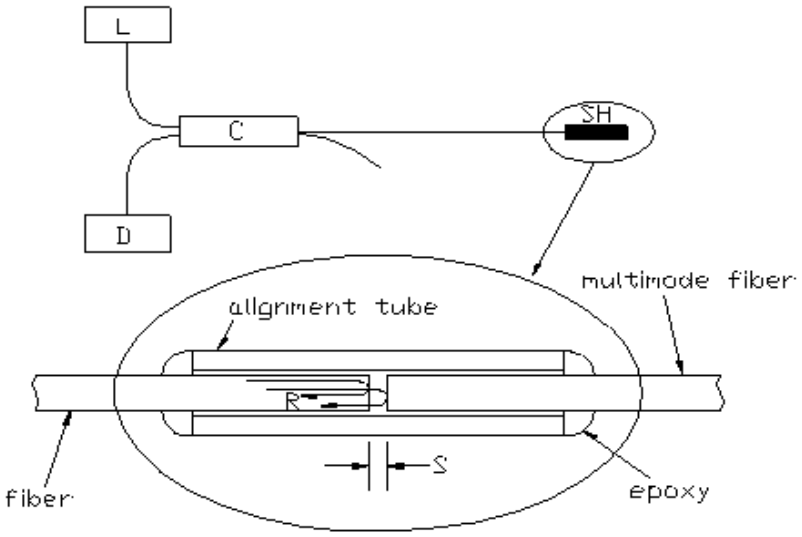

Figure 1.1. Traditional EFPI optical fiber sensor fabrication scheme.

In this research work, a sensor fabrication control system is investigated for EFPI sensor quasi-automated fabrication. This is the first attempt toward the long-term goal of automated

sensor fabrication. A high-energy carbon dioxide (CO_2) laser is for the first time used as the heating source to thermally fuse the silica fibers and tube for EFPI sensor fabrication. In the thermal bonding, quality, repeatability and formability are required. These are the great challenges in the automated thermal bonding process. Therefore, construction of a real-time control system is necessary. For the air gap separation control system, a white light interferometric subsystem is implemented for real-time monitoring and measurement of the air gap during the sensor fabrication. Several signal processing techniques are employed to improve the accuracy and resolution of air gap measurement. A set of user application software is developed for real-time control of a CO_2 laser power and pulse duration, a nanometer precision micro-motion stage, and a white light interferometric system. EFPI sensors fabricated using this system have shown excellent performance during high temperature and pressure tests.

1.3 Scope of Research

The objective of the research is to investigate a cost-effective, reliable and repeatable system for EFPI optical fiber sensor fabrication. Specifically, the issues listed below are considered in this research effort:

1. The initial air gap of the EFPI sensor needs to be accurately adjusted to a certain optimum value to meet the demand of our research work.
2. The initial sensor operating point needs to be precisely adjusted to the starting point of the linear portion of the interference fringe.
3. To achieve the best thermal stability, the capillary tube and the fibers must be permanently bonded together with a high mechanical strength.
4. Also the bonding should not have adverse effects on the optical properties of the fiber waveguide.
5. The sensor effective gauge length (the distance between the two bonding points) needs to be controlled within a tight tolerance so that the fabricated sensors have predictable and repeatable performances.
6. The fabrication of the sensor should be automatic or semiautomatic so that the sensor can be made in large quantities and at low cost.

Chapter 2 System Configuration

In the thesis research, we develop a system for controlled fabrication of Fabry-Perot sensors as shown in Figure 2.1. The system includes three subsystems, the functions of each subsystem are described below:

1) Carbon dioxide (CO_2) laser heating subsystem.

A high-energy CO_2 laser is used as the heating source to bond tube and fibers together. The CO_2 laser generates high-energy optical pulses at the wavelength of 10.6 μm. When the silica glass material is exposed to the CO_2 laser output, it absorbs the optical energy and converts it to thermal energy, which heats the silica glass materials locally up to very high temperatures.

2) Optical fiber white light interferometric subsystem.

The white light fiber optic interferometric subsystem is used for real-time monitoring and measurement of air gap separations in the Fabry-Perot sensor probes with a high resolution and accuracy.

3) X-Y translation stage/piezoelectric micro-motion positioning sub-system.

A nanometer precision X-Y translation stage and piezoelectric micro-positioning stages are used in the system for alignment of fiber with fiber and fiber with tube.

A host computer is used to control and coordinate these three sub-systems so that the CO_2 laser output power, the motion of the stages, and the sensor air gap measurement can be precisely controlled during the sensor fabrication process. Figure 2.2 shows the picture of the finished EFPI sensor fabrication control system.

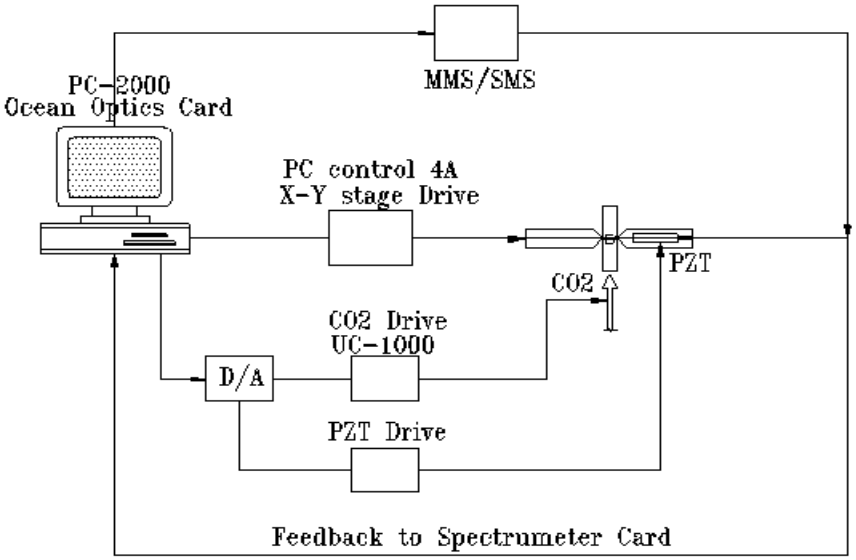

Figure 2.1. Scheme of controlled fabrication system of Fabry-Perot sensor.

Figure 2.2. Picture of controlled fabrication system of Fabry-Perot sensor.

2.1 CO_2 Laser Subsystem

The CO_2 laser used in the system is a *SYNRAD, Inc* Model 48-2 [18]. The wavelength emitted by the laser is 10.6 μm, and the maximum output optical power under continuous mode operation is 25 W. After using a cylindrical lens with a focal length of 7.5 inches, a spot size of about 300 μm wide and 3500 μm long can be achieved at the focal point. The laser can also be used to generate short optical pulses, which are externally modulated through a controller, with a minimum pulse duration of about 200 μs.

The control of the CO_2 laser output involves two parts: the power level control and the pulse duration control. The power level control can be accessed by externally applying a 0-10 V voltage signal (corresponding to 0-25 W output power) and the pulse duration can be controlled by inputting a standard TTL gating signal to enable or disable the laser output. Because it is necessary to precisely control the heating time and the temperature during the sensor fabrication, we designed and implemented a special circuit to allow computer programmable control of the CO_2 laser. The block diagram of the CO_2 laser control subsystem is given in Figure 2.3. By properly programming the DIO-24 interface card (National Instruments), the power control signal is sent out to the D/A circuit, which converts the digital signal to an analog output from 0 to 10 volts at a resolution of 16 bits as shown in Figure 2.4. This DAC is also used to control PZT motion which will be described in a later section. The laser enabling or disabling signal is also converted to a TTL gating signal through the same circuit.

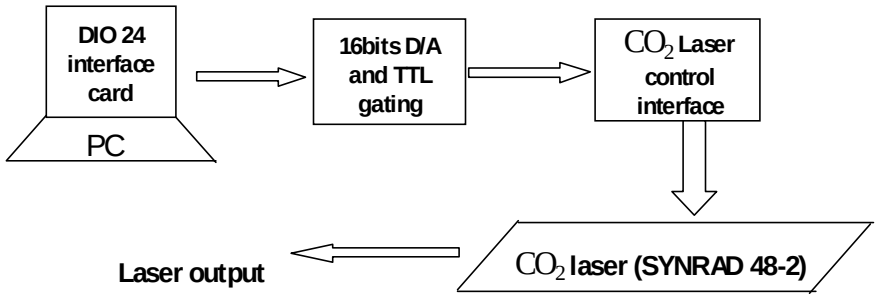

Figure 2.3. Block diagram of the CO_2 laser control subsystem.

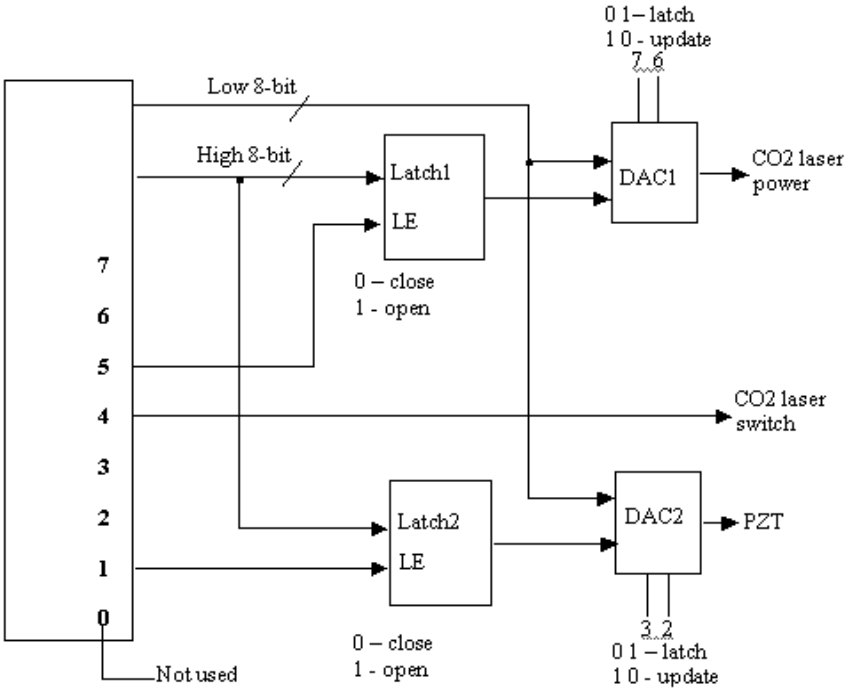

Figure 2.4. Diagram of DAC for CO_2 laser and PZT control.

2.2 Optical Fiber White Light Interferometric Subsystem

The use of optical interferometric techniques in optical fiber sensor applications allows access to the high resolution and large dynamic range. The white light interferometric technique uses low coherence, broadband spectral sources such as light emitting diodes (LEDs), multimode laser diodes or halogen lamps. Although this technique of optical fiber sensing was not reported until 1983, firstly for use with single mode fiber [18] and then with multimode fibers [19], its principle of operation had been demonstrated as a potential communication system in 1975 [20].

In the EFPI sensor fabrication control system, we use the white light interferometric subsystem to monitor in real-time and measure the air gap separation in the EFPI sensor. The measurement of the air gap separation is achieved by demodulating the interference spectrum of the sensor output as described in the section below. A set of software with graphic user

interfaces is developed for interrogation of a computer-compatible fiber spectrometer as part of the white light subsystem to determine in real-time the air gap separation in the Fabry-Perot sensors. Because we need to fabricate multimode and single mode fiber Fabry-Perot sensors, two white light interferometric air gap monitoring systems are constructed. The two systems share the same spectrometer but use different sources and fibers.

2.2.1 Principle of Optical Fiber White Light Interferometric Air Gap Monitoring

The basic principle of the white light interferometric air gap monitoring is illustrated in Figure 2.5. When the sensor is fabricated, two fibers with cleaved endfaces are inserted into a capillary tube. The partially reflected optical waves at these two endfaces will generate an

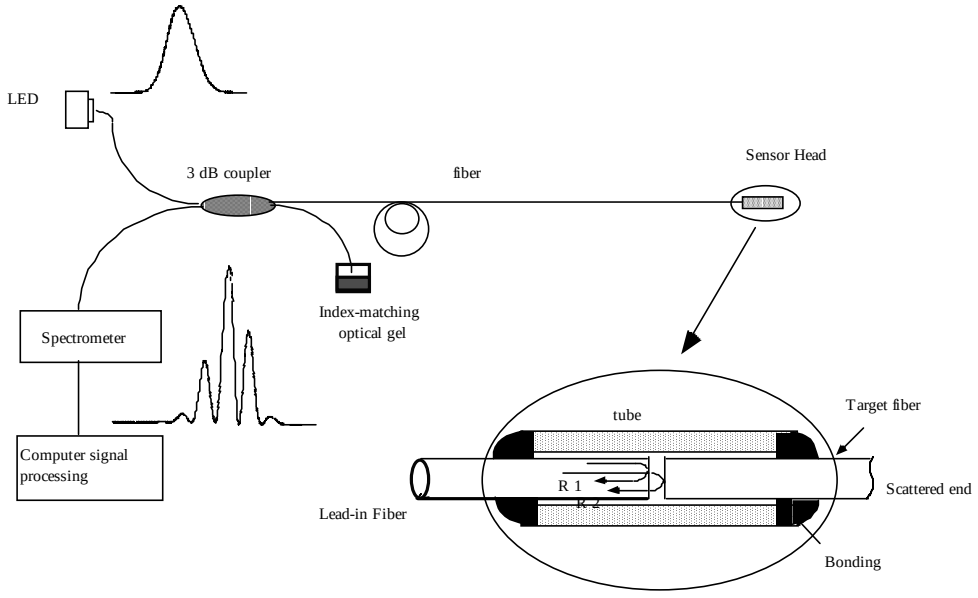

Figure 2.5. Principle of the white light interferometric air gap monitoring system.

interference signal which is transmitted back to the spectrometer through a 2x2 fiber coupler. We assume that the white light source (LED or SLD) has a near Gaussian spectral intensity distribution in its emitted radiation. Such a distribution can be described by the function

$$I_s(\lambda) = I_0 \exp\left[\frac{-(\lambda - \lambda_0)^2}{(\Delta\lambda)^2}\right] \qquad (2\text{-}1)$$

where λ_0 is the central wavelength, I_0 is the peak value, and $\Delta\lambda$ is the source spectral width. The output interference signal is then given by:

$$I = 2I_s(\lambda)k\left[1+\gamma(L)\cos\left(\frac{4\pi L}{\lambda}+\varphi_0\right)\right] \qquad (2\text{-}2)$$

Where the factor γ takes into account the decreased visibility due to the numerical aperture of the fiber as well as other attenuating effects, whose value is in the range of 0 ~ 1, k is the factor considering the effect of fiber loss and endfaces reflections, and φ_0 is the arbitrary initial phase difference between the two interference signals.

If we modify the interference spectrum given by Equation (2-2) with respect to the source spectrum, we have the normalized interference output expressed as

$$I_n = 2\left[1+\gamma(L)\cos\left(\frac{4\pi L}{\lambda}+\varphi_0\right)\right] \qquad (2\text{-}3)$$

It is shown in Equation (2-3) that the spectrum output by the sensor is modulated by a sinusoidal function due to the interference. Because the interference spectrum is a function of the sensor air gap length *L*, the successful demodulation of this spectral signal can render an accurate and absolute measurement of the sensor air gap length.

For each wavelength component, the difference in the phases of the two reflections from the sensor can be expressed as

$$\varphi_i = \frac{4\pi L}{\lambda_i}+\varphi_0 \qquad (2\text{-}4)$$

Thus the phase difference between two spectral components is given by

$$\Delta\varphi = \varphi_1 - \varphi_2 = \frac{4\pi L(\lambda_2-\lambda_1)}{\lambda_1\cdot\lambda_2} \qquad (2\text{-}5)$$

Rewriting Equation (2-5), we have

$$L = \frac{\Delta\varphi\cdot\lambda_1\cdot\lambda_2}{4\pi(\lambda_2-\lambda_1)} \qquad (2\text{-}6)$$

If the phase difference for these two spectral components is known, the absolute value of the sensor air gap separation *L* can be calculated by Equation (2-6).

Although it is not easy to measure the phase difference for two spectral components, there exist a few special points with fixed phase relation. For example, the phase difference between two adjacent peaks (or valleys) is 2π. Therefore, by detecting the spectral locations of the peaks or valleys in the interference spectrum, we can obtain the cavity length *L* by applying Equation (2-6).

2.2.2 Relationship Between Air Gap Measurement Error and Wavelength Measurement Error

Consider two adjacent peaks or valleys, the air gap can be determined absolutely by Equation (2-7). The relationship between air gap measurement error and wavelength measurement error is derived as follows:

In Equation (2-6), if $\Delta\varphi$ is set to be 2π, we then have

$$L = \frac{\lambda_1 \lambda_2}{2(\lambda_2 - \lambda_1)}, \qquad (2\text{-}7)$$

and further $$|\Delta L|^2 = |\frac{\partial L}{\partial \lambda_1}\Delta\lambda_1|^2 + |\frac{\partial L}{\partial \lambda_2}\Delta\lambda_2|^2, \qquad (2\text{-}8)$$

or $$|\Delta L|^2 = |\frac{-2L^2}{\lambda_1^2}\Delta\lambda_1|^2 + |\frac{-2L^2}{\lambda_2}\Delta\lambda_2|^2 \qquad (2\text{-}9)$$

Assuming there is a sensor with air gap separation $L = 8\mu m$, $\lambda_1 = 800nm$, and $\lambda_2 = 840nm$, and the wavelength measurements for λ_1 and λ_2 have the same error, then the air gap measurement error ΔL is approximately $270\Delta\lambda$. We can see that a $0.1nm$ wavelength measurement error can cause an error of about $27nm$ in the air gap measurement. So using two adjacent peaks or valleys to calculate the air gap is very sensitive to wavelength measurement error $\Delta\lambda_1$.

Now we rewrite Equation (2-4) to be:

$$\frac{4\pi L}{\lambda_i} = 2\pi m_i. \qquad (2\text{-}10)$$

or $$m_i = \frac{2L}{\lambda_i} \ . \qquad (2\text{-}11)$$

For a fixed air gap separation L, each peak or valley wavelength λ_i corresponds to a certain integer number m_i. From Equation (2-11), we get:

$$L = \frac{m_i}{2}\lambda_i, \quad \text{and} \quad \Delta L = \frac{m_i}{2}\Delta\lambda_i \qquad (2\text{-}12)$$

Assume there is a sensor with air gap separation $L = 8.0\mu m$ and $\lambda_1 = 800nm$, then m_1=20, so $\Delta L = 10\Delta\lambda_1$. As a result, if we only trace one peak or valley to measure air gap separation, $0.1nm$ measurement error only causes only $1.0nm$ air gap measurement error. But tracing one peak or valley is a relative measurement of air gap separation. We must first determine an air gap separation and then to find the peak or valley which we decide to trace. To achieve absolute measurement and a high resolution simultaneously, we combine the above two methods together: first find all peaks and valleys positions, calculate an initial air gap separation, and then get the specified value m for the valley which is the nearest to central wavelength 850 nm. By tracing this valley within a dynamic range, we can measure the air gap separation with a resolution as high as 0.1 nm.

2.2.3 Implementation of Multimode and Single mode Fiber White Light Subsystems

Two white light subsystems were designed and constructed to support the control of the EFPI sensor fabrication. One is designed for fabricating multimode fiber Fabry-Perot sensors, and the other is for single mode fiber sensors. The two subsystems share the same spectrometer but have different sources, couplers, and fibers.

The spectrometer used in the white light subsystem is a fiber optic PC plug-in spectrometer whose schematic is shown in Figure 2.6 (PC2000 manufactured by Ocean Optics, Inc.). The PC2000 spectrometer card uses a 1200-line holographic grating to diffract the input light to a CCD array, and interfaces with the computer using a 12 bit A/D through the ISA bus [21]. The blaze wavelength is 850 nm, and the best efficiency is from 750 nm to 950 nm, which covers the whole light source spectrum of interest. The resolution of this spectrometer is approximately 0.3 nm, and the highest data acquisition speed is 1MHz.

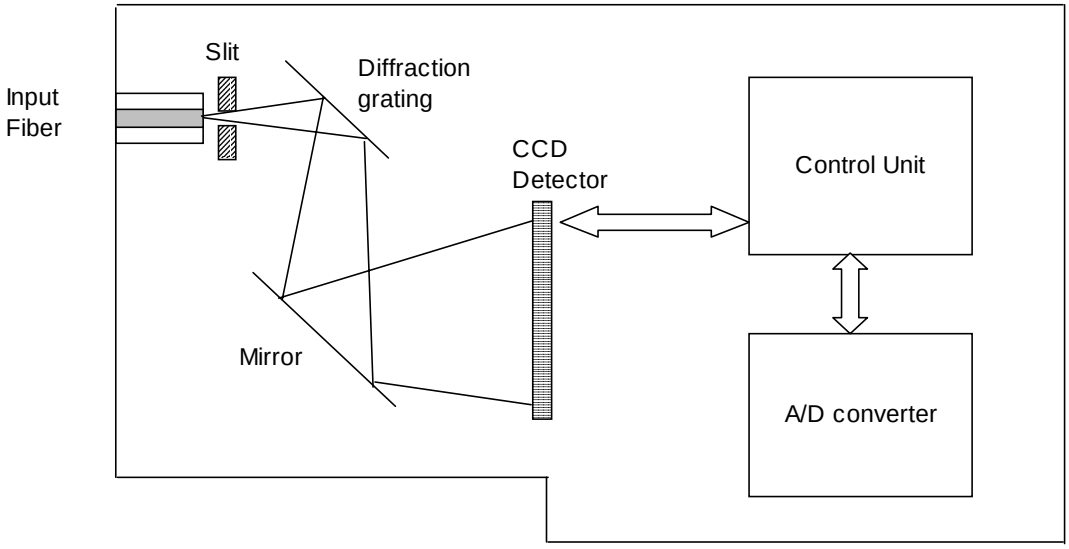

Figure 2.6. Principle of spectrometer card.

2.2.3.1 Multimode Fiber White Light Air Gap Monitoring System

Multimode fiber sensors offer a number of general advantages over single mode fiber sensors such as simplicity and low cost in their basic form, so they are potentially attractive for cost effective, bulk applications [20]. Broadband light sources suitable for coupling light in fibers generally have relatively large dimensions, so large core fibers can be employed, which improves tolerances with respect to end effects and so facilitates interconnections.

Multimode fiber interferometric sensors have less sensitivity than single mode fiber equivalents. However, this is frequently not a problem for industrial measurements. Multimode fiber temperature sensors, for example, manufactured through this sensor fabrication control system in the Photonics Laboratory at Virginia Tech, have a resolution on the order of 0.1^{o} C.

The configuration of the multimode fiber white light air gap monitoring system is shown in Figure 2.7. The light source is an LED (Honeywell HEF 4857-014) with a central wavelength

of 850 nm and spectral width of 74 nm. The fiber used is a standard multimode graded index 62.5/125 telecom fiber. The picture of the system is shown in Figure 2.8.

2.2.3.2 Single mode White Light Air Gap Monitoring System

Single mode fibers are used for sensing when extreme sensitivity is required or when a well defined polarization of light is needed at a remote sensing point. Most sensors which use single mode fibers are of the intrinsic type [10]. However, they have also been designed as the extrinsic type in the past decade [22].

In practice, single mode fiber sensors tend to need very stable, highly coherent sources with low phase noise in order to gain full advantage of their potential sensitivity. When such sources are used, absolute calibration of phase difference is normally not possible and a range limit arises from the periodic nature of the interferometer output. However, both of these problems can be avoided by using sources emitting in a broad wavelength range, with some compromise regarding the ultimate sensitivity achievable with any particular sensor [3].

In this research work, the single mode fiber white light air gap measurement system has a larger dynamic range than the multimode fiber system. The configuration of the single mode fiber white light air gap monitoring system is shown in Figure 2.9. We use a superluminscent diode (SLED form EG&G Inc.) with a central wavelength of 1310 nm and a spectral width of 40 nm as the source. A Temperature controller employing a thermoelectric cooler (TEC) is also used to stabilize the source temperature. The fiber used inside the system is a standard 9/125 single-mode telecom fiber. The picture of the system is shown in Figure 2.10.

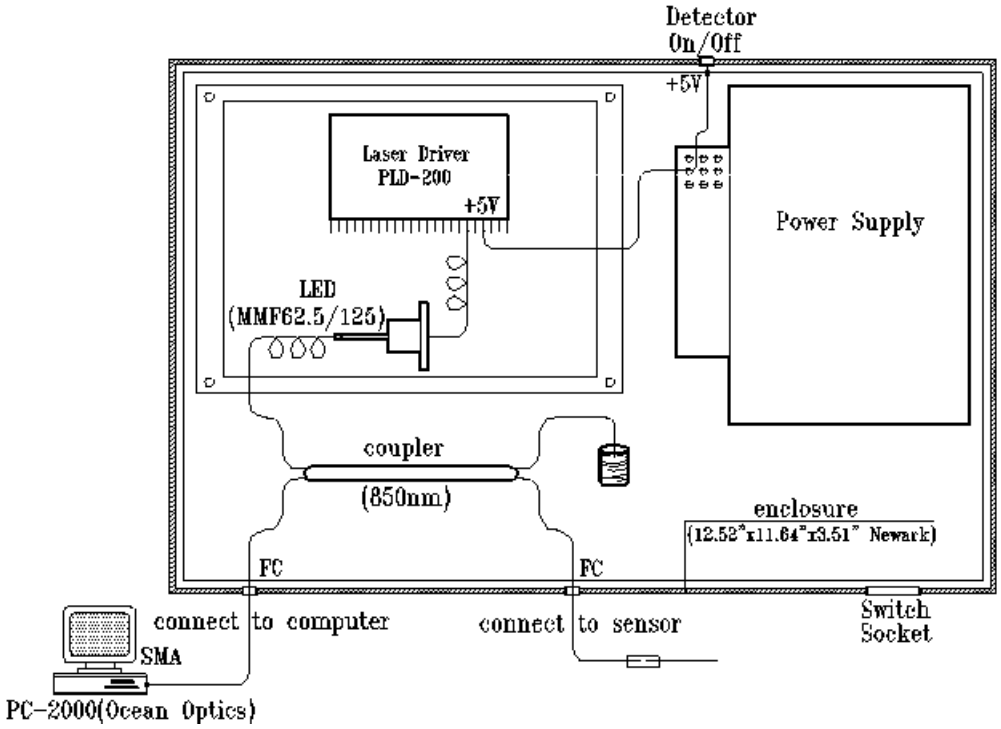

Figure 2.7. Configuration of the multimode fiber white light air gap monitoring system.

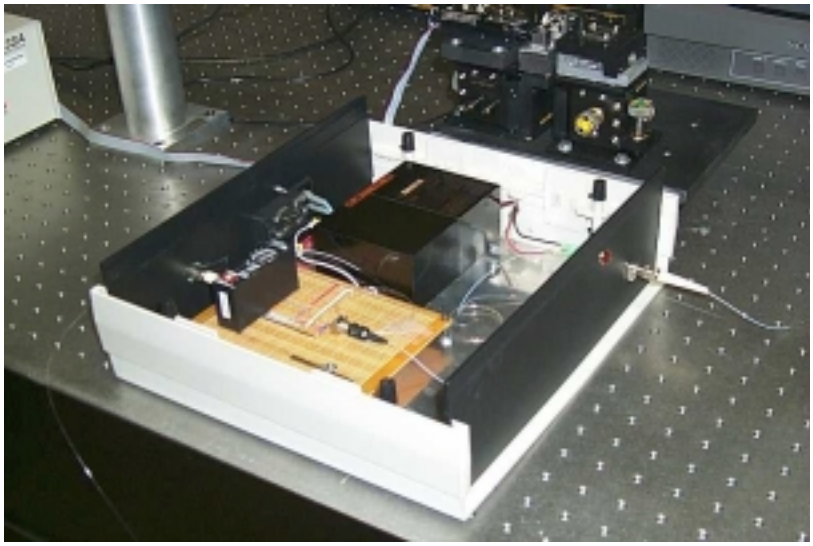

Figure 2.8. Picture of the multimode fiber white light air gap monitoring system.

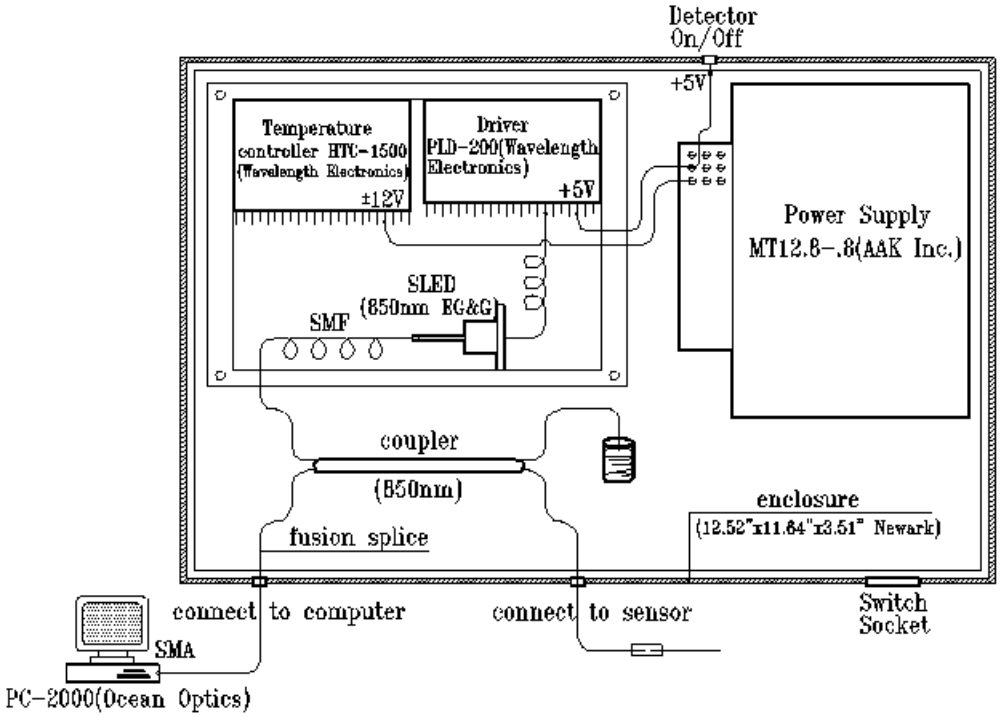

Figure 2.9. Configuration of the single mode fiber white light air gap monitoring system.

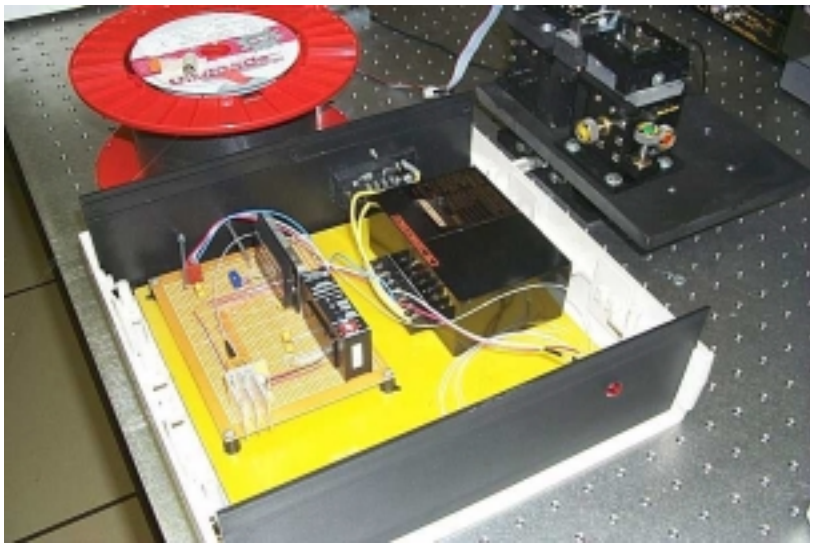

Figure 2.10. Picture of the single mode fiber white light air gap monitoring system.

2.3 X-Y Translation Stage/Piezoelectric Micro-motion Positioning Subsystem

During the sensor fabrication, the fibers and the capillary tube must be kept precisely aligned. The sensor air gap needs to be accurately adjusted to the preset value, and the bonding distance, which determines the sensor effective gauge length, also needs to be precisely controlled. Therefore it is necessary to design a fiber positioning system for the sensor fabrication to accurately position the fibers and the tubes.

The computer controlled micro-motion fiber and tube positioning system is illustrated in Figure 2.11. The two fibers are positioned on two V-grooves using magnets, and the V-grooves are each fixed to a 3-dimentional translation stage, respectively. Between the two translation stages, a supporting block with another V-groove on top is used to position the capillary tube. All the V-grooves are specially designed and manufactured to hold the fibers or the capillary tube tightly. After installation, the three V-grooves are precisely aligned to fall in a straight line so that there is no offset angle during sensor fabrication. Fibers can be inserted into the central capillary tube by moving the two translation stages in three dimensions. To allow precise adjustment of the sensor air gap length, another small PZT-actuated stage is used to move the target fiber with ultra-high resolution along y-direction. The movement of the stage is controlled by the central computer through a PZT driver and a 16 bits D/A circuit as shown in Figure 2.4. In order to control the sensor gauge length, a big translation stage is used to move the whole setup in two directions with respect to the CO_2 laser beam. After the tube is bonded to the lead-in fiber, this stage can precisely position the second bonding point with respect to the CO_2 laser beam. A video microscope system is used to help the aligning procedure and to monitor the whole sensor fabrication process. The picture of the sensor fabrication stage system is shown in Figure 2.12.

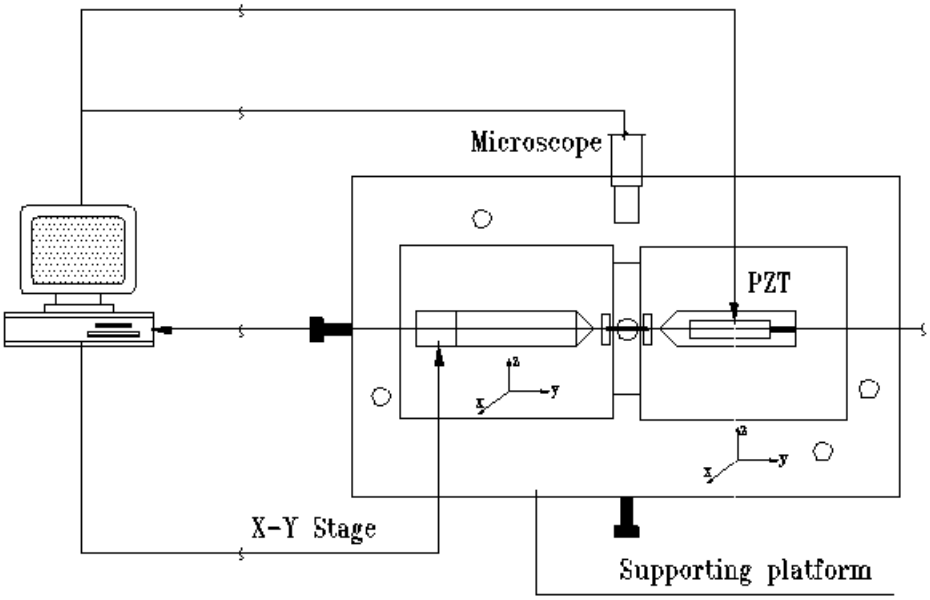

Figure 2.11. Computer controlled micro-motion fiber and tube positioning system.

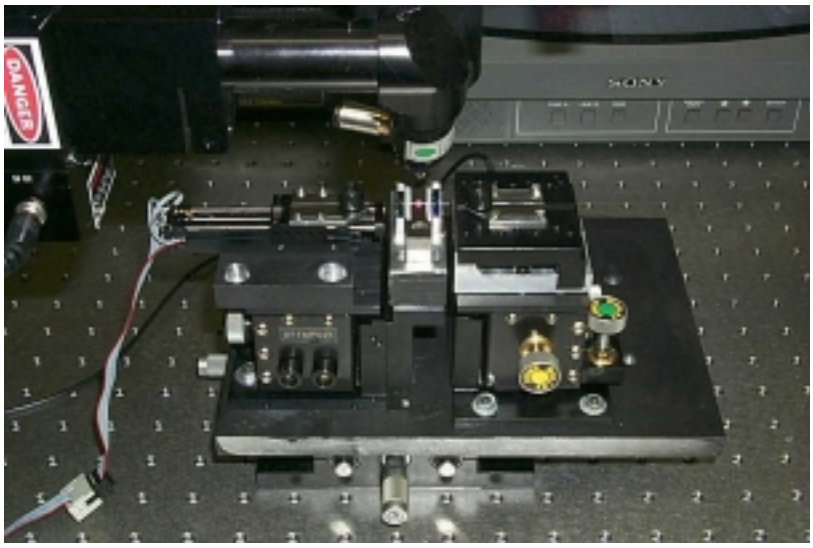

Figure 2.12. Picture of the sensor fabrication stage system.

Chapter 3 Software Design for Sensor Fabrication Control System

3.1 Scheme of System

A host computer has played an important role in the sensor fabrication control system. The computer is a system controller and interfaces with users. It controls in real-time a CO_2 laser as the energy source for the sensor thermal bonding, an X-Y translation stage and a PZT micro motion for the fiber to fiber and fiber to tube alignment, and a white light interferometric system for air gap separation monitoring and measurement. A set of application software is designed to ensure the sensor fabrication with high performance, low cost, and good repeatability. Friendly graphic user interfaces also enable users with minimal training to easily perform the complicated sensor fabrication work.

The application software is developed based on object-oriented programming (OOP) with Visual Basic 6.0. The hierarchy of the software structure [23] is shown in Figure 3.1. Object-oriented programming has many advantages over procedure programming. It provides reusability, flexibility, and extensibility. The code of functions can easily be used with other programs; the code of functions can easily be modified without affecting the user interface; and some new functions can easily be added into the system [24]. The tree diagram of user menu functions is shown in Figure 3.2. Some complicated mathematic functions such as FFT are written in C language as dynamic linked library (DLLs). The software includes three subsystems in accordance with the hardware:

1) CO_2 laser control subsystem for real-time control of CO_2 laser power and pulse duration to provide accurate laser energy for tube and fibers thermal bonding.

2) White Light interferometric subsystem for monitoring and measurement in real-time of the air gap separation in Fabry-Perot sensors. It requires a fast response and ultra-high accuracy.

3) Micro-motion fiber positioning subsystem for off-line fiber to fiber and fiber to tube alignment before bonding and for real-time adjustment of the air gap separation to the desired value with nanometer precision.

To achieve the control of sensor fabrication, we must integrate the three subsystems into one system that becomes a closed-loop. The work principle follows three steps: first, two fibers

and a hollow tube are set up on the X-Y stage, through the X-Y off-line control sub-system to align the sensor. Second, the air gap separation is monitored in real-time through the white light interferometric subsystem. Finally, when the air gap reaches the initial value, a CO_2 laser control subsystem is started up to effect thermal bonding of the fiber and tube, at the same time a PZT control subsystem is used to adjust in real-time the air gap error caused by thermal expansion and other factors. The flowchart of the system operations is shown in Figure3.3.

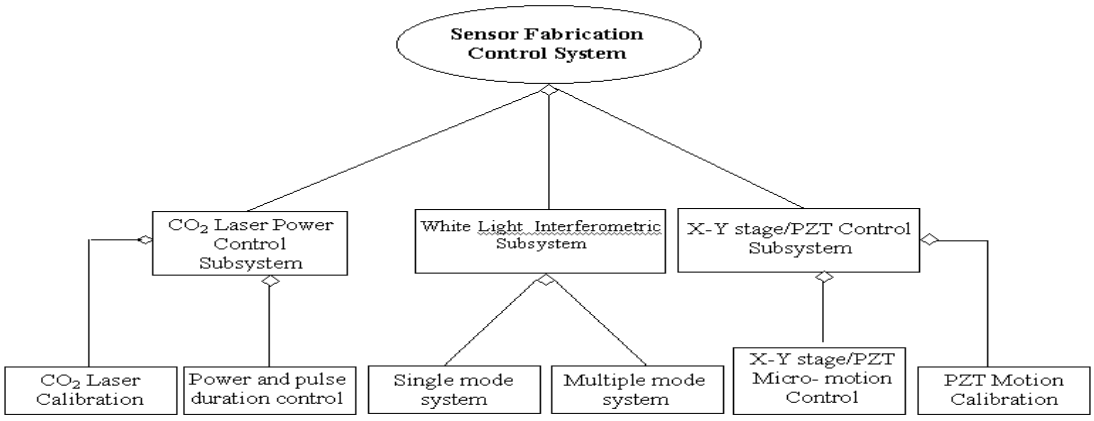

Figure 3.1. Hierarchy of the software structure.

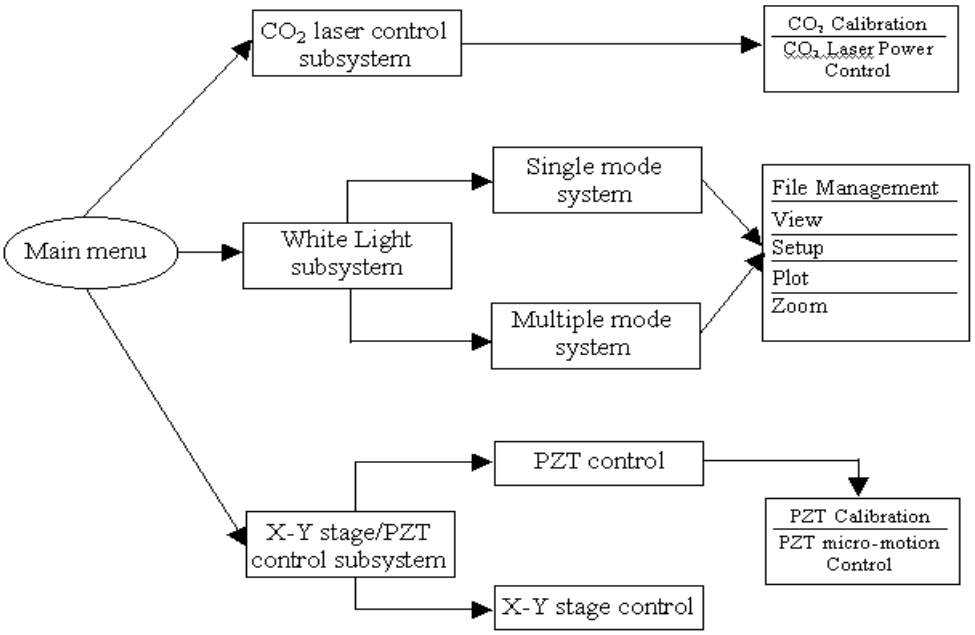

Figure 3.2. Tree diagram of user menu functions.

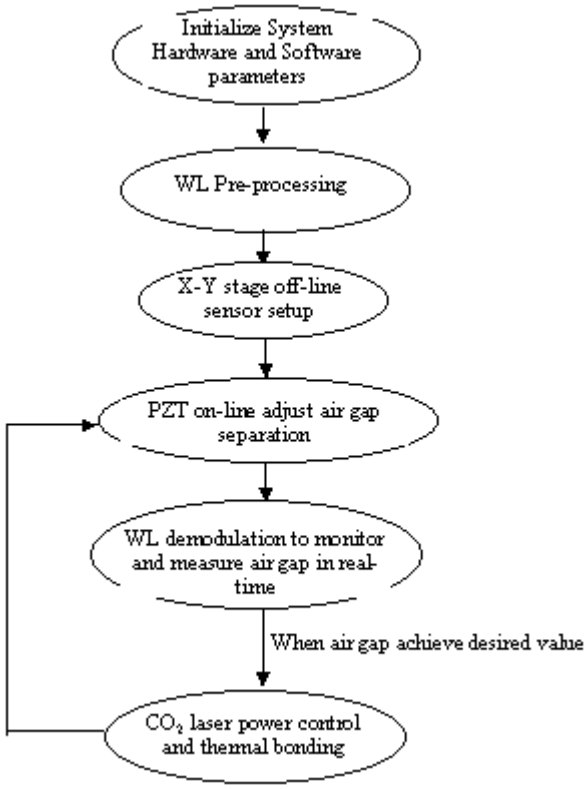

Figure 3.3. Flowchart of the system operations.

3.2 CO_2 Laser Control Subsystem

The CO_2 laser is used as the heating source during the sensor fabrication. It is important to control the laser output power and exposure duration accurately to ensure solid bonding between the fibers and the tube. Too large laser power and too long exposure time can result in degradation of the optical properties of the optical fiber and the too much stress at the bonding region. On the other hand, too weak laser power or too short exposure time can result in incomplete bonding. The previous version of CO_2 laser control software was written in C on the CVI LabWindows platform. In order to integrate the three subsystems into one system, this part of the code was rewritten in Visual Basic 6.0.

3.2.1 CO_2 Laser Calibration

The CO_2 laser power is controlled by computer software via a D/A converter. As mentioned in Chapter 2, the output voltage from the 16-bit D/A card is in the range of 0-10V

corresponding to CO_2 laser power 0-25Watts [25]. But the CO_2 laser output is quite non-linear when it is controlled through the external analog port. To achieve precise control of the output power, we conducted a calibration experiment for the CO_2 laser. The laser output power was measured using a power meter. The results are plotted as shown in Figure 3.4. Based on the calibration data, the CO2 laser power can be accurately mapped to the external control voltages. Thereafter, precise control of the laser output power can be realized through curve-fitting method.

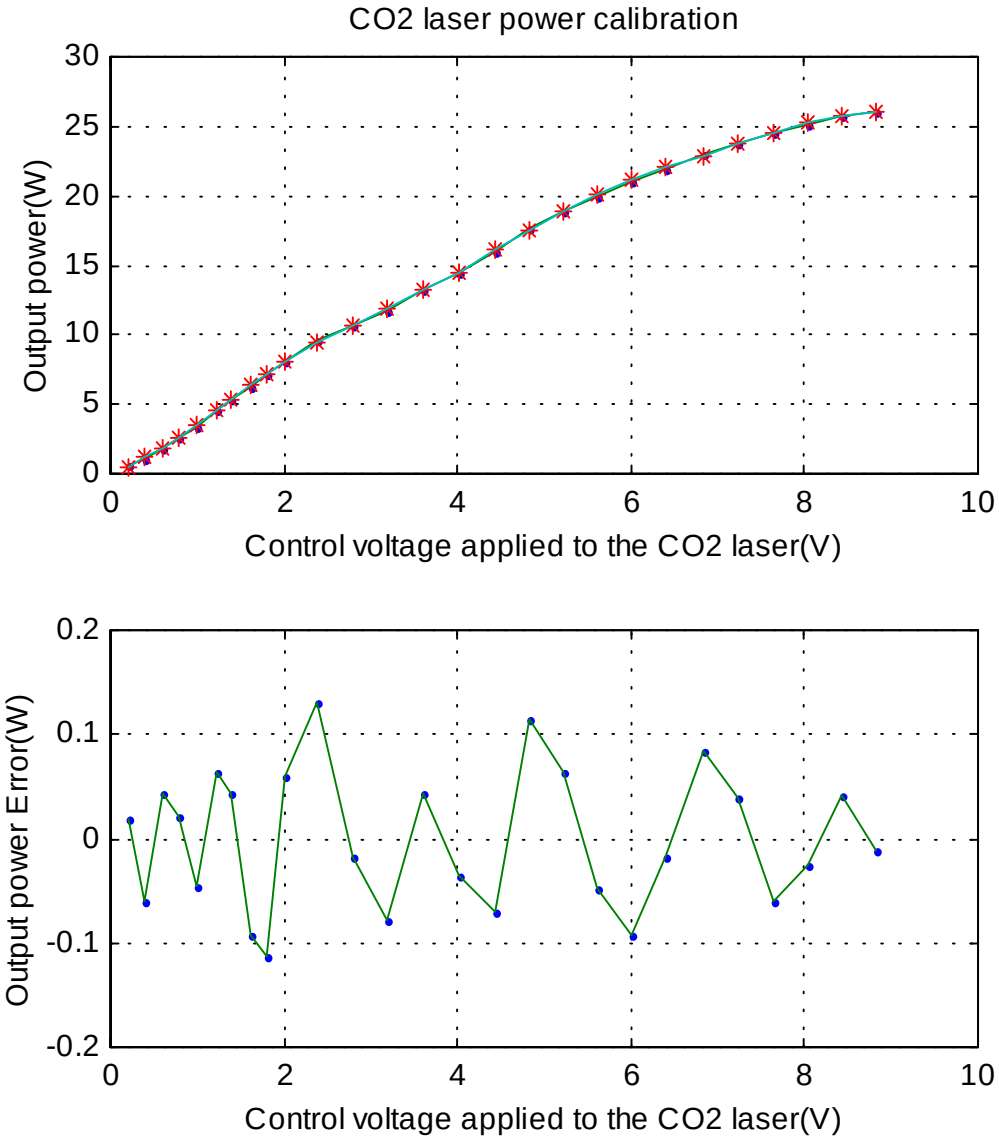

Figure 3.4. CO_2 laser output power calibration results.

3.2.2 CO_2 Laser Power and Pulse Duration Control

In order to achieve the best optical and mechanical performance of the fabricated sensor, we choose the power curve which is shown in Figure 3.5. t_1 time is given for pre-heating the tube and fiber before the laser power is raised to full power P_3. At the same time, this t_1 period will clean up possible dust grains accumulation on the surface of the tube through high temperature burning. It can allow the full powers bonding with the time duration of ($t_2 - t_1$) we need to use in thermal bonding of the glasses. The time duration of ($t_3 - t_2$) is an annealing time, which ensures the tube without being broken due to a sudden temperature reduce after bonding and eliminates the residual stresses in the sensor. The optimum values of these parameters have been obtained through experiments, which will be reported and discussed in Section 4.2. A user interface shown in Figure 3.6 is designed to set up the parameters.

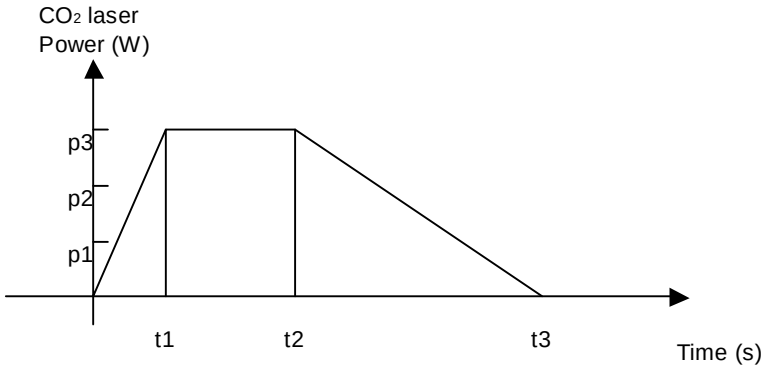

Figure 3.5. Curve of CO_2 laser power level and exposure time.

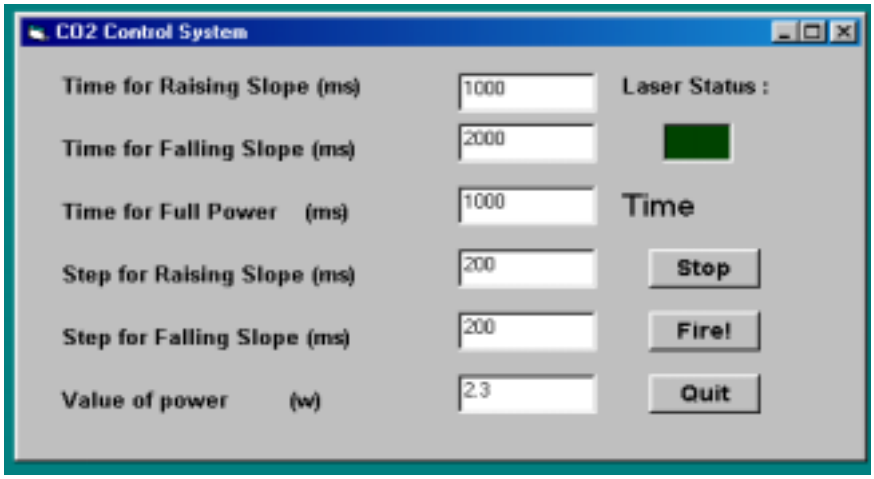

Figure 3.6. User interface of CO_2 laser power control subsystem.

3.3 White Light Interferometric Subsystem

The white Light interferometer subsystem is one of the most important subsystems in the controlled sensor fabrication system. Providing high frequency and accurate real-time air gap monitoring and measurement is the main goal of this subsystem. Several signal processing methods are studied. Application software with a set of graphic user interfaces is designed for interrogation of the computer-compatible fiber spectrometer as part of the white light subsystem to determine in real-time the air gap separation in the Fabry-Perot sensors.

3.3.1 Classical Digital Spectral Analysis Method

Classical spectral analysis is to utilize the Fourier transform as a mathematical foundation for relating a time or space signal to its frequency-domain representation. Using the FFT algorithm, the air gap separation of a Fabry-Perot sensor is determined by identifying the frequency of the sinusoidal period in the wave number $(1/\lambda)$ domain. This periodicity corresponds uniquely to a specific air gap based on the constructive and destructive super positioning of individual wavelengths. Applying an FFT results in a spectral peak corresponding to a specific value in the frequency domain. This peak falls within a single FFT bin which correlates to an air gap [26].

With this spectral analysis, the resolution is directly related to the record length. It would seem logical that we would want to calculate the FFT with as large of a record length as possible by increasing the zero-pad. With a long record of 524288, the theoretically estimated resolution as high as 1nm can be achieved. However, the computation time and hardware memory requirements would not be practical. For example, it takes 4.2 seconds to compute a complex FFT of 2^{17} (131072) elements using a 133 MHz Pentium processor [27]. The computation alone would also require 2 MB of memory to store and execute the transform. Clearly from the practical standpoint of speed, increasing the record length of the data via zero padding to improve the resolution of the spectral estimation is not a viable option. Another important thing is using FFT spectral analysis can easily measure larger air gap separation such as a few hundred microns. It is usually difficult to measure such smaller air gap separation as a few microns.

Another signal processing scheme is to use a curve fitting algorithm to determine the peak position of the digitized fringe pattern output of a white light interferometric system [28]. This method is to fit a cosine function to the normalized fringe. The cosine function y (x) is given by

$$y(x) = a\cos[4\pi(x - x_0)/\lambda_a] + b \qquad (3\text{-}1)$$

Then, by adjusting the value of a, λ_a, b, x_0, the sum of squares for error (SSE) can be minimized. The SSE is given by

$$SSE = \sum_i (I[i] - y(X[i]))^2 \qquad (3\text{-}2)$$

But the curve fitting method is more suitable for fixed air gap separation of the sensor. We investigate a more efficient method for dynamic air gap monitoring and measurement which is described in the following section.

3.3.2 Peak Tracing Method for Signal Processing in White Light Subsystem

Advanced computer software was developed to demodulate the interference spectral signal output from the white light subsystem so that the air gap separation in the sensor can be dynamically monitored with high accuracy while the sensor is fabricated. The computer software is based on the previously discussed phase detection method in Chapter 2 in which peaks and valleys in the interference spectrum are detected. The software is implemented in a combination of Visual Basic and C languages so that both graphic interfaces and high computational speed are achieved and optimized. The block diagram of the white light subsystem is shown in Figure 3.7. In the measurement processing, the user can repeatedly change some of the parameters settings and the software will generate results corresponding to the latest setting. The user interface of the designed software is shown in Figure 3.8 as a single mode type and Figure 3.9 as a multimode type. The major functions of this software include:

- ***Initialization***

The program begins with the system hardware initialization, including initialization of the spectrometer, output of the CO_2 laser, initial position of the X-Y translation stage, and PZT driver. The program automatically saves all the parameters of the last experiment. So the software parameter initialization will keep the latest settings.

- ***Pre-processing***

The main purpose of this part is to improve the signal-to-noise ratio (SNR) of the system for accurate air gap length measurement.

1) The dark spectrum is the dark current output of the system without input signal to the system. It is saved to allow only pure spectral data to be processed after the subtraction algorithm.

2) The original spectrum of the light source which is shown in Figures 3.8 (a) and 3.9 (a) is saved as the reference so that the interference spectrum can be normalized to eliminate the distortions induced by the source spectrum.

3) A boxcar algorithm is developed to filter and smooth the raw data so that the noise of the spectrometer is minimized.

4) The interference spectrum is automatically truncated according to its signal level. This ensures that only the high SNR region of the spectrum is included in calculations of the air gap separation.

- ***Demodulation***

This part includes the most important functions of the software.

1) The saved dark spectrum is subtracted from the input spectrum, and the saved reference spectrum is used to normalize the interference spectrum so that the source spectrum effects are eliminated, as shown in Figure 3.8 (c) and 3.9 (c).

2) An FFT algorithm is used to automatically estimate the window size of the interference spectrum. This allows an optimal number of data points to be used in Step 3).

3) Coarse locations of the peaks and valleys are found by a smart comparison algorithm. These coarse locations are used as reference marks in the demodulation.

4) Cutting levels for each peak and valley are determined by setting 1/3 difference intensity of adjacent peak and valley.

5) A mass-centroid algorithm is applied to find the interference peaks (or valleys) and the corresponding wavelengths.

6) Coarse air gap separation is obtained according to Step 5) and Equation (2-7).

7) The feature number m for the valley nearest to central wavelength can be given according to Step 6) and Equation (2-10).

8) Tracing this valley to monitor and measure air gap separation in the sensor.

9) When the traced valley moves out of the truncated window, the next valley will be traced, its feature number m is obtained by adding 1to the previous m automatically.

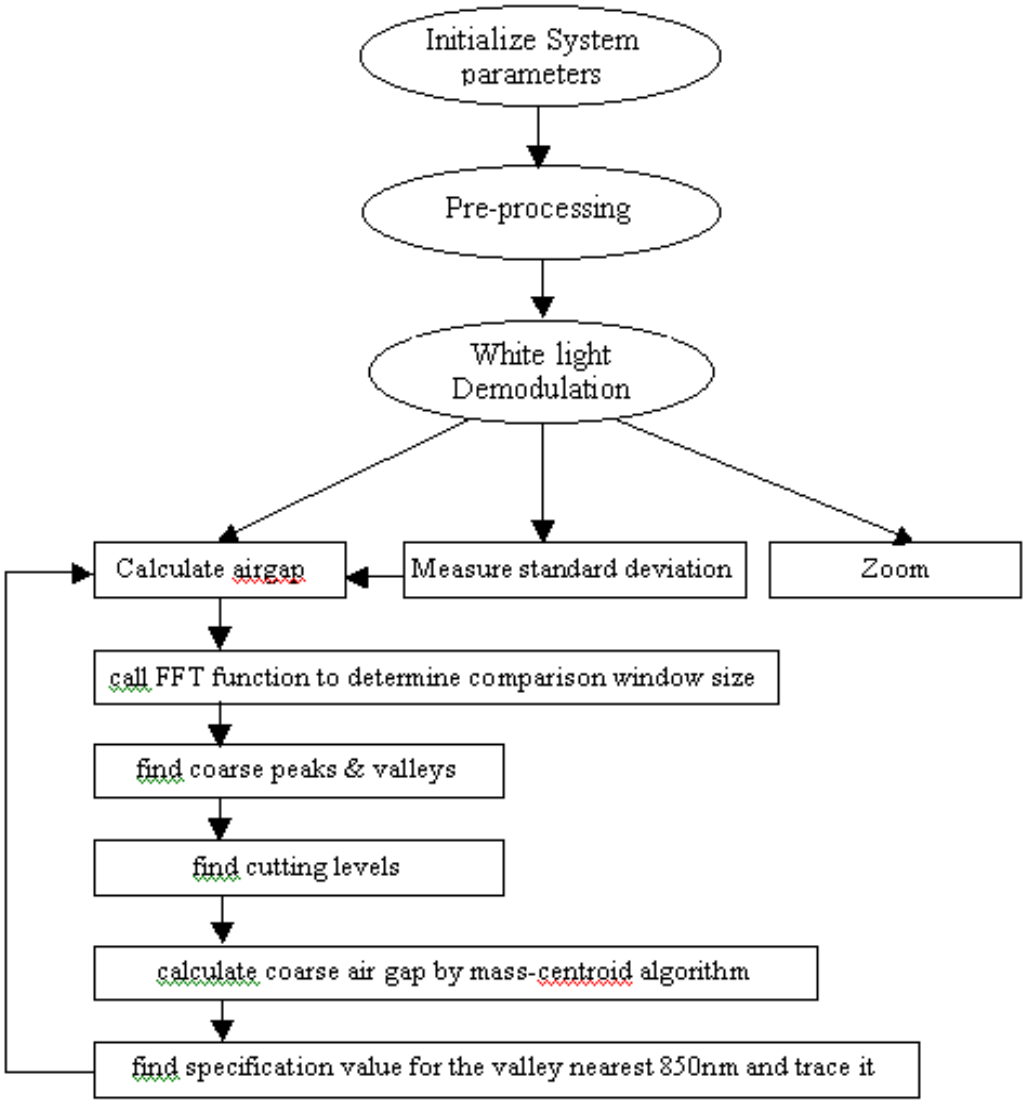

Figure 3.7. Block diagram of the white light interferometric subsystem.

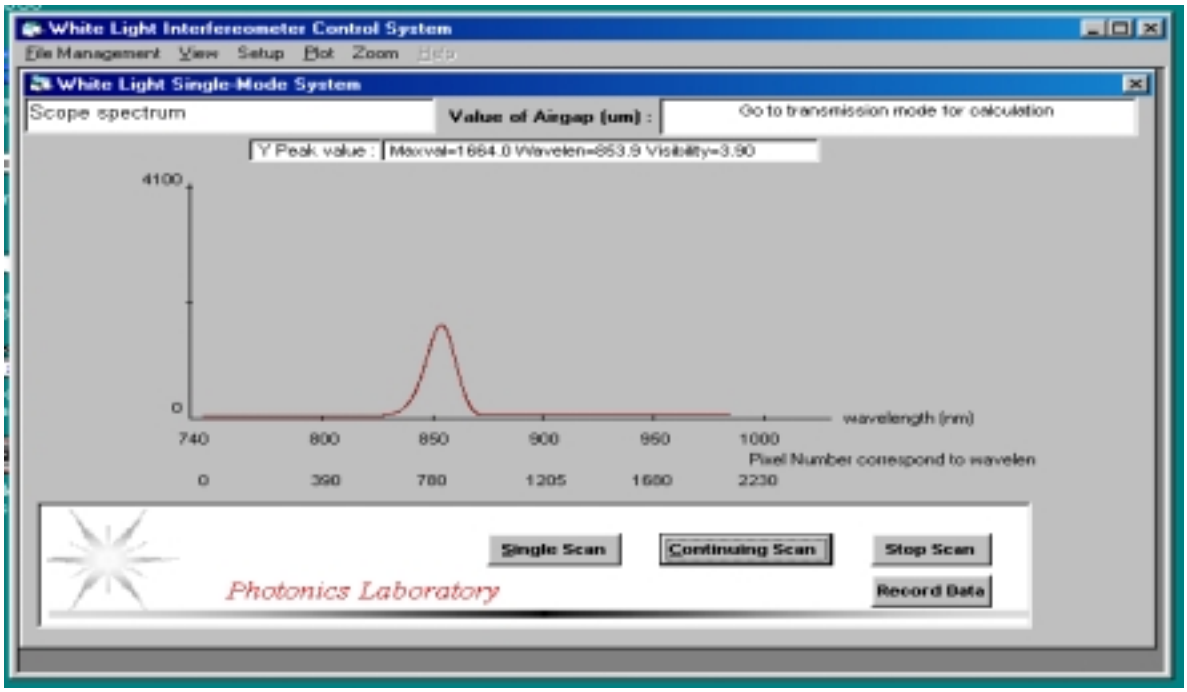

(a) Source spectrum of Single mode fiber sensor.

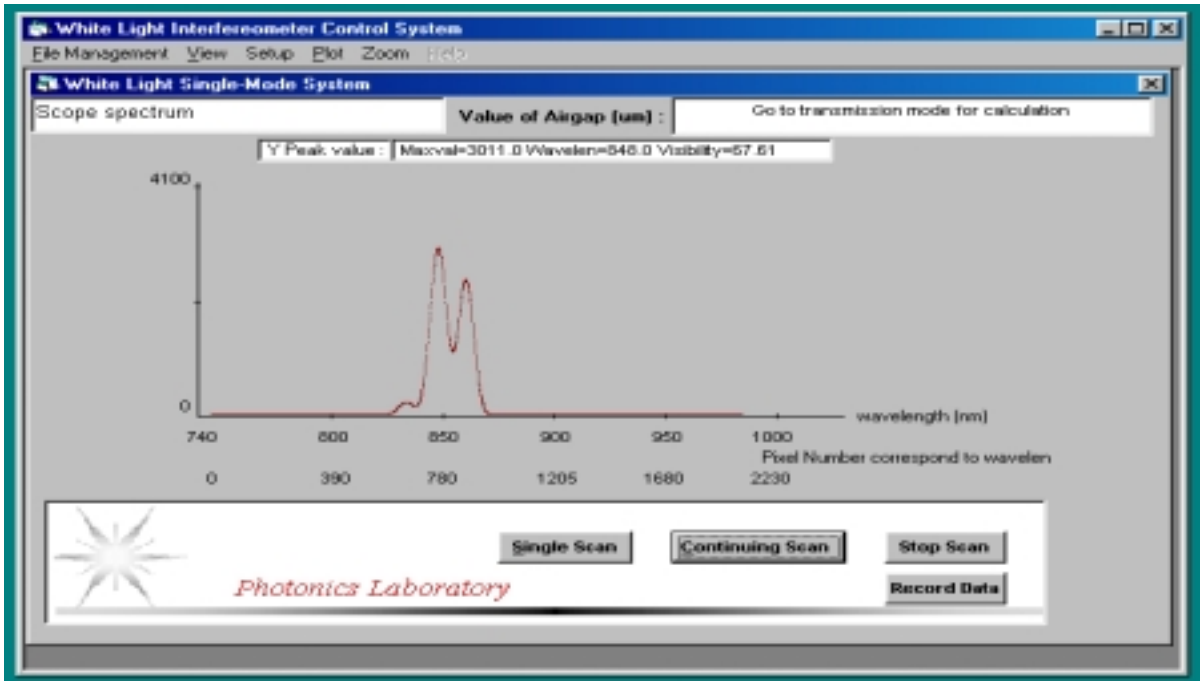

(b) Scope spectrum of Single mode fiber sensor.

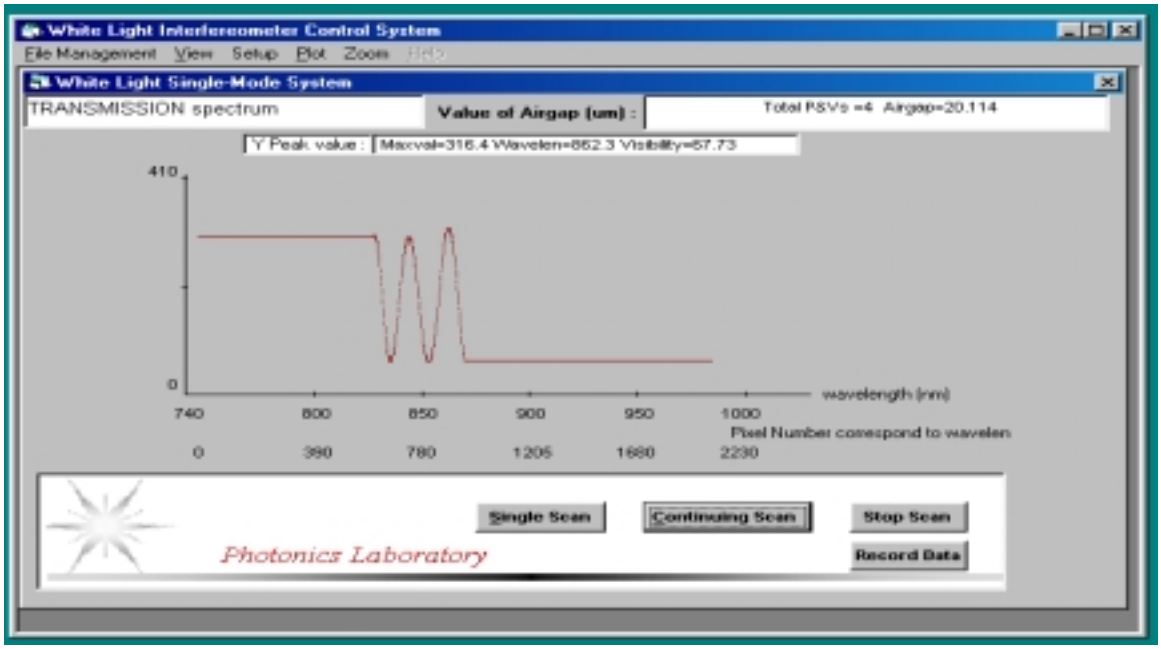

(c) Transmission spectrum of Single mode fiber sensor.

Figure 3.8. Spectrum of single mode sensor under the white light subsystem and GUI.

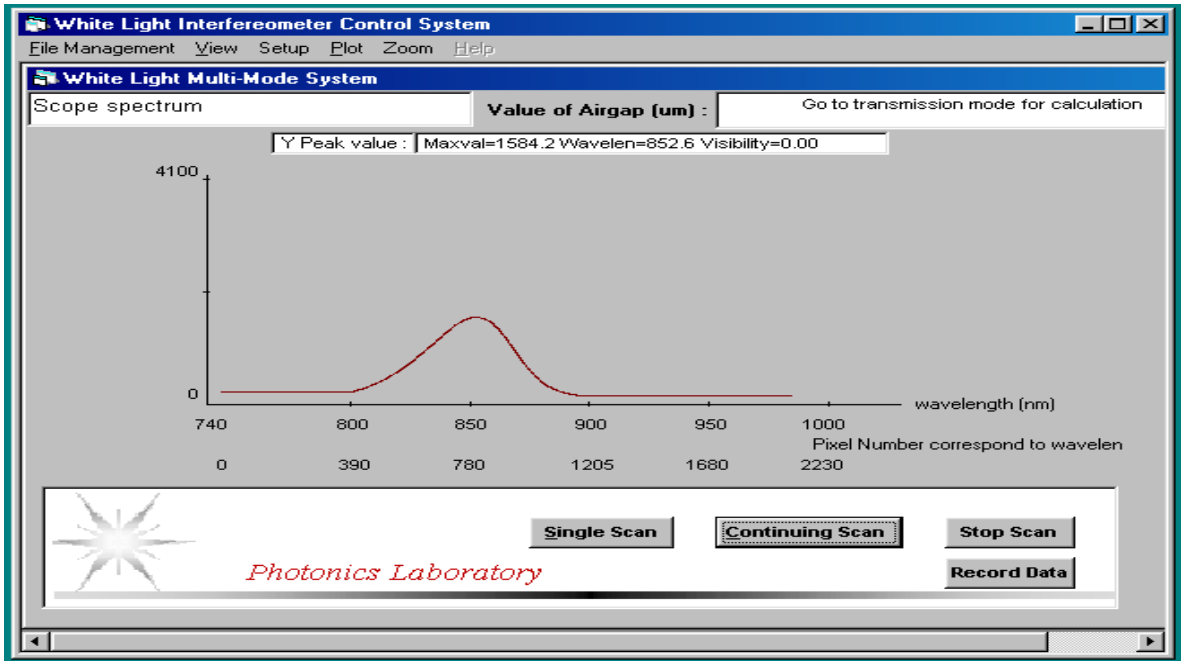

(a) Source spectrum of multimode fiber sensor.

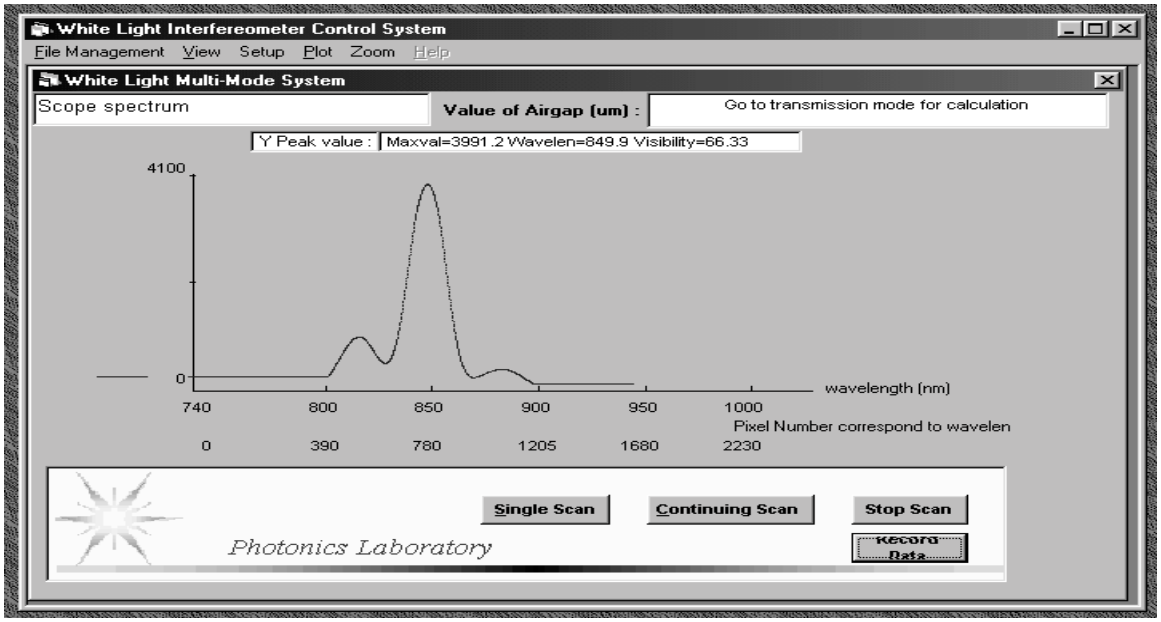

(b) Scope spectrum of multimode fiber sensor.

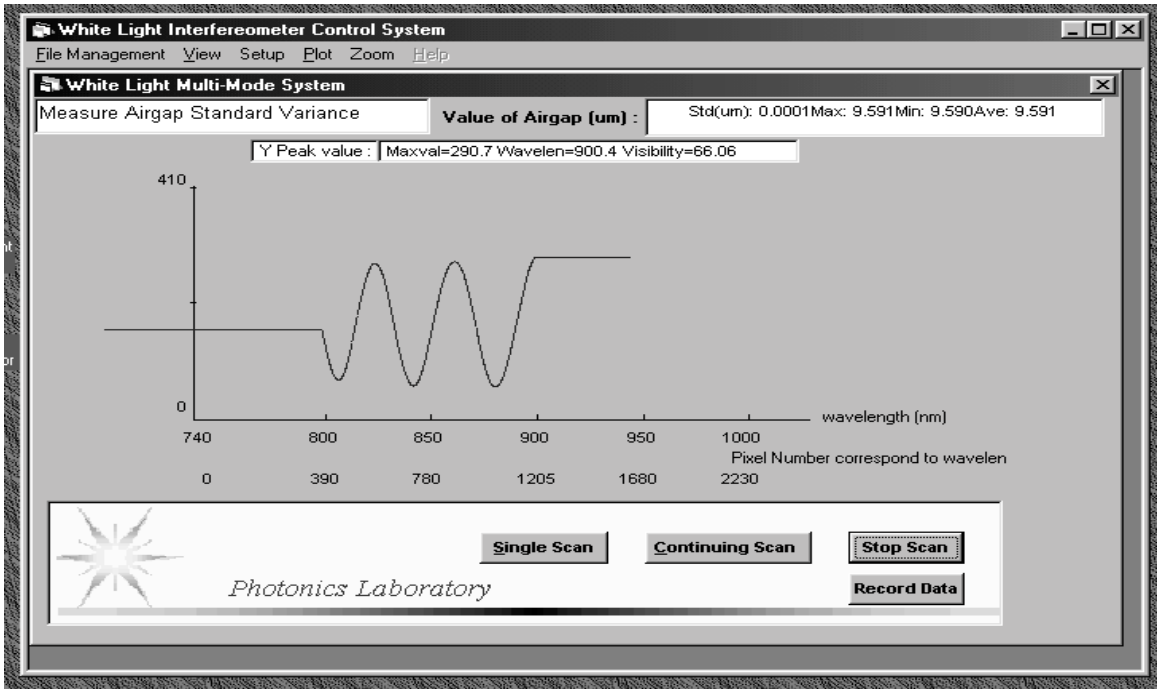

(c) Transmission spectrum of multimode fiber sensor.

Figure 3.9. Spectrum of multimode sensor under the white light subsystem and GUI.

3.4 Micro-motion Fiber Positioning Subsystem

The significance and basic principle for micro-motion fiber positioning subsystem have been described in Chapter 2. In this subsystem, a servo X-Y translation stage and a piezoelectric (PZT) micro stage are employed. Two sets of software are designed to control the motion of each.

3.4.1 X-Y Translation Stage Control Software

The X-Y translation stage is used to control off-line the alignment of fiber with fiber and fiber with tube. The motion range is about 15mm. The program receives the required motion value in microns and converts it into counts. Then the program calls the library functions to drive the stage move. Figure 3.10 represents the flowchart of the X-Y translation stage control software, and Figure 3.11 shows the user interface of the X-Y Translation Stage control software. The main functions of the X-Y translation stage control software includes:

- Initialize board ID and set system velocity and acceleration.
- Set X or Y axis required motion values in microns.
- Reset the stage position to the initial value.
- Report motion status and current positions.
- Start motion and Stop motion

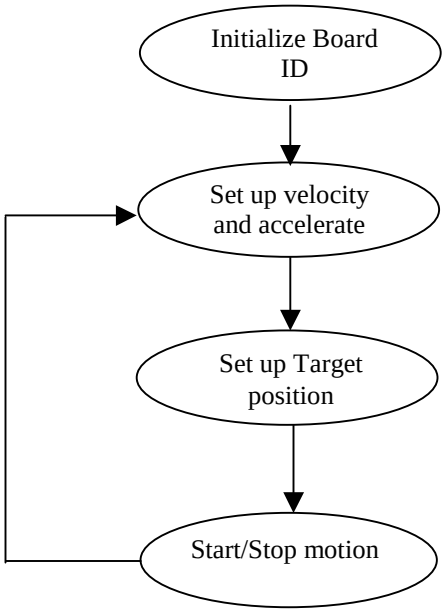

Figure 3.10. Flowchart of the X-Y translation stage control software.

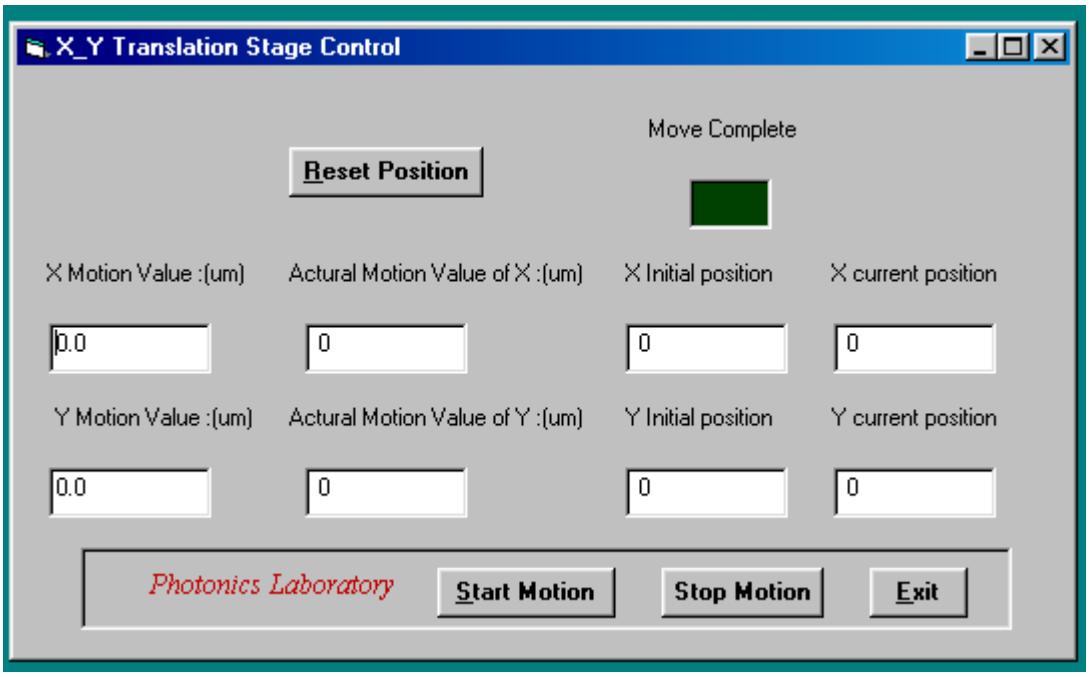

Figure 3.11. User interface of the X-Y translation stage control software.

3.4.2 Piezoelectric (PZT) Control Software

a lead zirconate titanate (PZT) piezoelectric actuator is used to control and adjust in real-time the air gap separation in the sensor. It is a high accuracy micro-motion stage. The motion of the PZT actuator is controlled by the host computer through a 16-bit D/A converter. The output voltage from 16-bit D/A card is in the range of –5V to +5V corresponding to a PZT movement range of –5 to +5um[29]. This DAC is integrated with that of the CO_2 laser (shown in Chapter 2, Figure 2.4). Computer software is designed to realize user interface and control function. The software reports the current air gap value in microns. A user can input the desired air gap value. When CO_2 laser is on, the PZT system will keep tracking of the air gap measured from the white light system and real-time adjust the air gap to a desired value. Figure 3.12 represents the Flowchart of the PZT control software. Figure 3.13 shows the User Interface of the PZT control software. The main functions of the PZT control software includes:

- Calibrate the PZT.
- Report current air gap measured from the white light interferometric subsystem.
- Set the desired air gap separation.

- Report motion status and,
- Start motion.

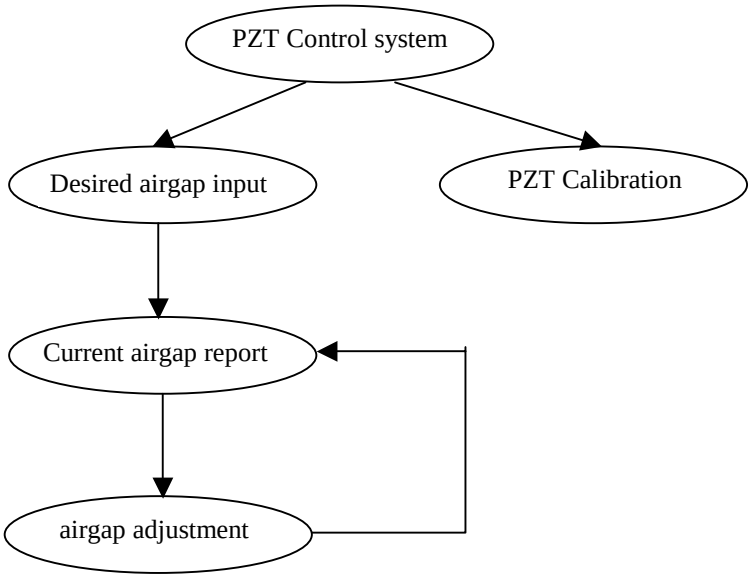

Figure 3.12. Flowchart of PZT control software.

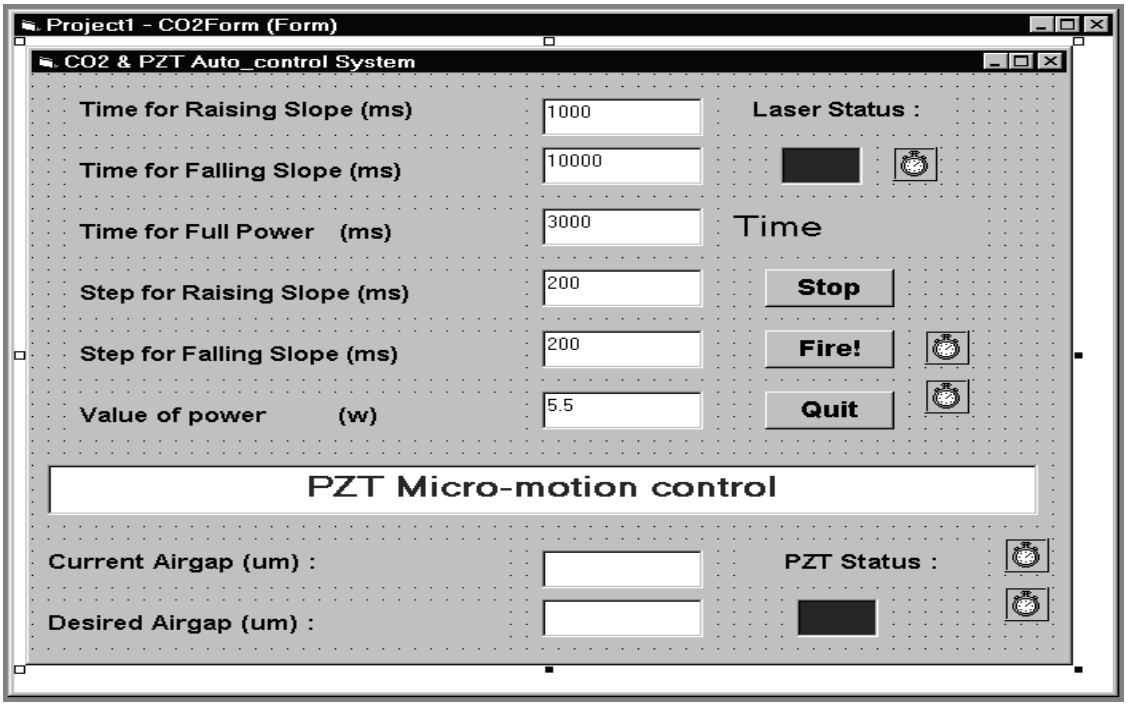

Figure 3.13. User interface of PZT control software.

Chapter 4. Experiments and Results

A large number of sensors have been fabricated using the implemented Fabry-Perot sensor fabrication control system. The main purpose of the sensor fabrication is two-fold:

1) To verify the design and to check out the functions of each subsystem;
2) To fabricate SCIIB sensors for further evaluation.

4.1 White Light Interferometric Subsystem Performance Test and Results

The purpose of designing the white light interferometric subsystem is to achieve real-time monitoring of the sensor air gap separation during sensor fabrication. There are several key performance characteristics that are required to be tested before it can be used. These include the accuracy, resolution, dynamic range, and frequency response of the air gap separation measurement.

4.1.1 White Light Interferometric Subsystem Calibration -- Accuracy

The accuracy of a measurement system is the extent to which the output deviates from that of a calibrated standard. Thus although accuracy is related to the resolution of the system, the accuracy will in general be poorer than the resolution.

Before the sensor fabrication control system is used, determination of the accuracy for the white light interferometric subsystem is very important. The subsystem is calibrated and tested through the use of a helium-neon (He-Ne) laser as the source and an Oscilloscope connected to the transmission end of a sensor while the reflection is still connected to the white light interferometric subsystem. The calibration system is setup as shown in Figure 4.1. Two signal demodulation methods were used to measure the air gap separation of the multimode fiber EFPI sensor. A white light source (LED) is used to inject the light to the interferometer, and its interferometric spectrum is demodulated by the spectrometer so that the absolute value of the air gap of the EFPI sensor is given. From another coupler, a He-Ne laser was used to input the light to the interferometer and a silicon photodetector was used to monitor the interference signal of the sensor. A narrow band optical filter centered at 633nm with a bandwidth of 10 nm was used in front of the photodetector so that the light from the

LED at the opposite end of the interferometer is filtered out. The transmitted light from the He-Ne laser has the wavelength of 633 nm which does not fall into the receiving spectrum range of the spectrometer so that the two signal demodulations do not interfere with each other. The change of the air gap can be measured both by counting fringes generated by the He-Ne laser and by processing the white light interferometric spectrum. These two measured results can be compared precisely as shown in Figure 4.2. X-axis represents the air gap calculated from the oscilloscope trace; Y-axis represents the air gap measured with the white light system. Figure 4.3 shows the deviation of the two methods within the air gap for a range from 5μm to 21μm. The deviations between these two signal demodulations are smaller than ±10nm [30]. Note that this also includes the measurement error of the He-Ne laser interferometry whose accuracy is limited because of the change of the coupling of the laser power to the fiber, the change of the fiber attenuation, and the limited resolution of the digital oscilloscope used in the experiment. The combination of these practical effects usually limit the resolution of the fringe counting interferometry to about 1/10 of one interference fringe which in this case is about 15 nm.

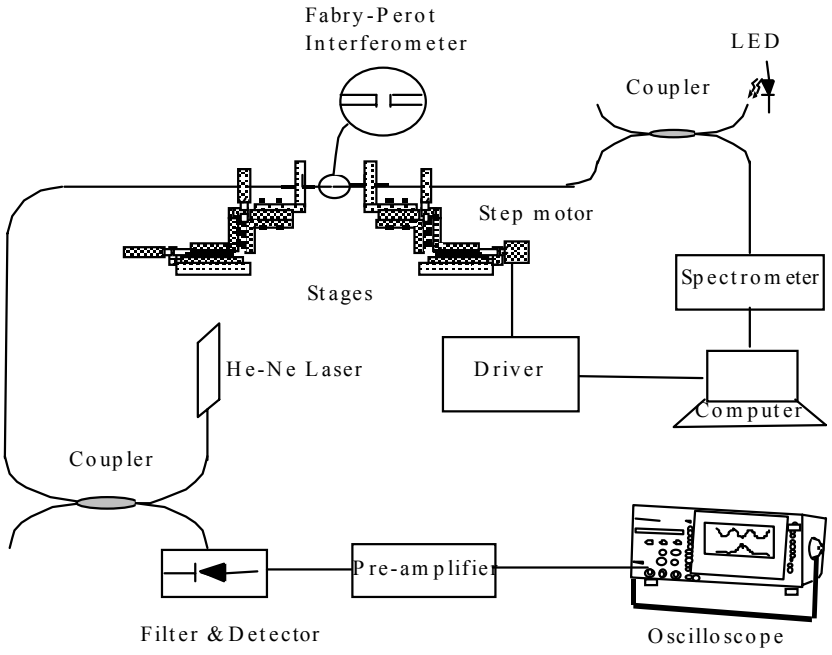

Figure 4.1. White light interferometric subsystem calibration setup.

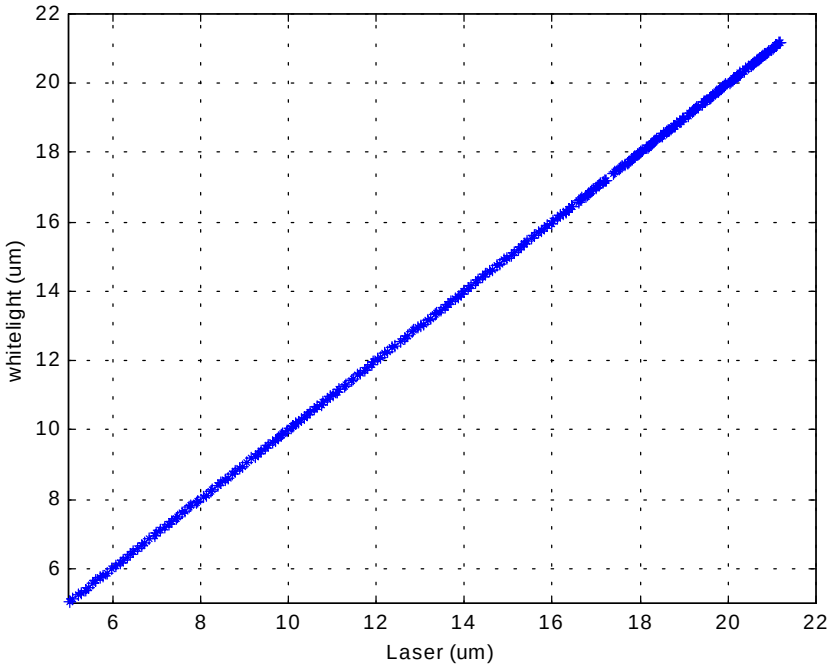

Figure 4.2. White light interferometric subsystem calibration.

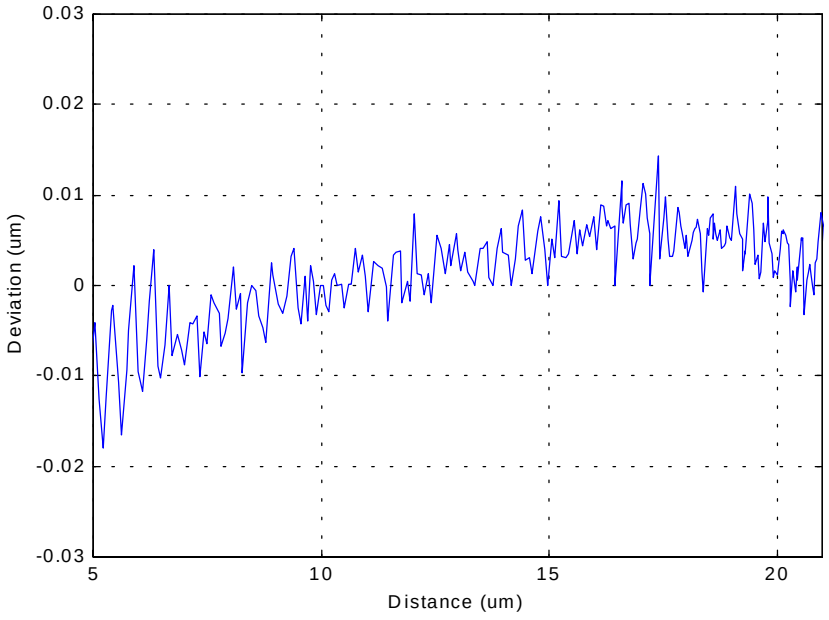

Figure 4.3. White light interferometric subsystem calibration deviation.

4.1.2 Standard Deviation of Air Gap Measurement

Standard deviation is a quantity that indicates measurement resolution of the white light interferometric subsystem. It is measured by fabricating a fiber optic extrinsic Fabry-Perot interferometric (EFPI) sensor with a fixed air gap. We use the white light interferometric subsystem to measure the EFPI sensor air gap 1000 times. Based on the measurement results, we can calculate the standard deviation of the white light interferometric subsystem. Actually, this function is built in the software so that we can perform the standard deviation measurement at any time. The standard deviation for both multimode and single mode fiber white light air gap measurement subsystems are calculated to be $\sigma = 0.0001$ μm but have different dynamic measurement range, which is described in Section 4.1.4.

4.1.3 Frequency Response Test

Since we need to monitor in real-time the air gap separation when we fabricate sensors, enough air gap measurement frequency response is required. Regardless of the hardware, the air gap measurement frequency response is related with sampling frequency, plot mode, curve fitting window size and sampling delay time. In our software, all these parameters can be set by users. The host computer used is a 400 MHz Pentium processor. The fastest sensor air gap calculation time under the PLOT mode is less than 0.1 seconds. Therefore, the corresponding frequency response of the system is higher than 10 Hz. According to our experiment, the average thermal bonding time of the EFPI sensor is about 4 seconds, and this time is determined by the CO_2 laser power ramp curve which will be described in Section 4.2. As a result, the frequency response of the white light interferometric subsystem is sufficient.

4.1.4 Dynamic Range of White Light Interferometric Subsystem

As described in Chapter 2, the air gap separation of the sensor can be measured through the white light interferometric subsystem. However, the air gap measurement range is not unlimited. The smallest air gap is that the fringe appeared in the calculation window must has at least one peak and one valley. The air gap can be calculated via Equation (2-6). The largest air gap measured value is dependant on the fringe visibility. We change the air gap by pulling the second reflection endface apart from the first one. Because the light through

the first endface is diffused, when the light intensity of the first endface is fixed, the larger the air gap, the smaller the reflection light intensity, and the poorer the fringe visibility. So there is a work dynamic range of the air gap for a good sensor. On the other hand, the air gap separation should be within the coherent length of the sensor. The coherent length is reversely proportional to the source spectrum $\int\lambda$. Because the $\int\lambda$ of single mode fiber white light system is smaller than that of the multimode fiber white light system, the air gap measurement range of single mode fiber system is larger than multimode fiber system.

The white light interferometric subsystem has two applications. One is small range measurement of air gap separation, usually within one fringe. Another application is large range measurement. For the multimode fiber system, this full dynamic range from 4 μm to 20 μm can be achieved and for the single mode fiber system the full dynamic range from 8 μm to 70 μm can be achieved. The standard deviation of the sensor air gap measurement is constant over the whole dynamic range. The typical initial air gap for multimode fiber sensor is about 6 μm and 15 μm for single mode fiber sensor. Therefore, the dynamic ranges of the white light interferometric subsystem for both systems are large enough.

Figure 4.4 demonstrates the air gap measurement performance within a small dynamic range of 0.4 μm. We placed a multimode fiber sensor with an air gap of 9.591μm into an oven and increased the temperature from room temperature to 1400^{o} F with 50^{o} F each step. The upper plot of Figure 4.4 shows the air gap change is linear to temperature. The lower plot of Figure 4.4 shows the error when using linear curve to fit the experiment points. For this sensor, the error is about 0.2%.

For testing the performance of large dynamic range measurement, we put a multimode fiber sensor with an air gap separation of 9.038μm and a gauge length of 8mm into the Automated Pressure Control System (APP) pressure sensor calibrator and increased the pressure from 0psi to 6000psi with 200psi each step. The sensor response is shown in Figure 4.5. During the test, there are 5 valleys moved out of our truncated window. The program traces one valley after another when the first valley is moved out of the window. In the

lower plot of Figure 4.5, there is about ±5nm deviation of the air gap measurement which corresponds 0.6% percent deviation in the whole measurement range.

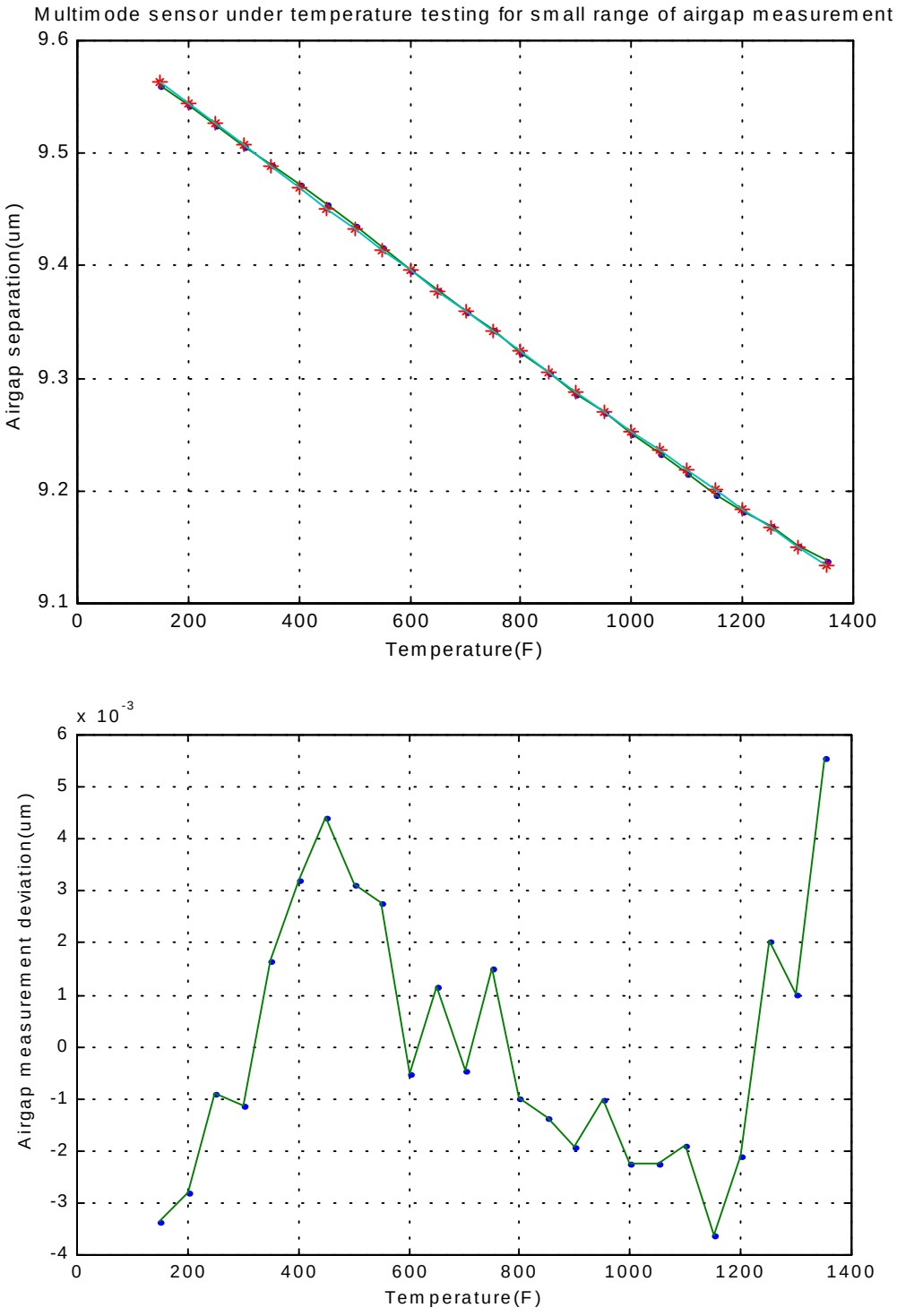

Figure 4.4. Air gap measurement performance in small dynamic range.

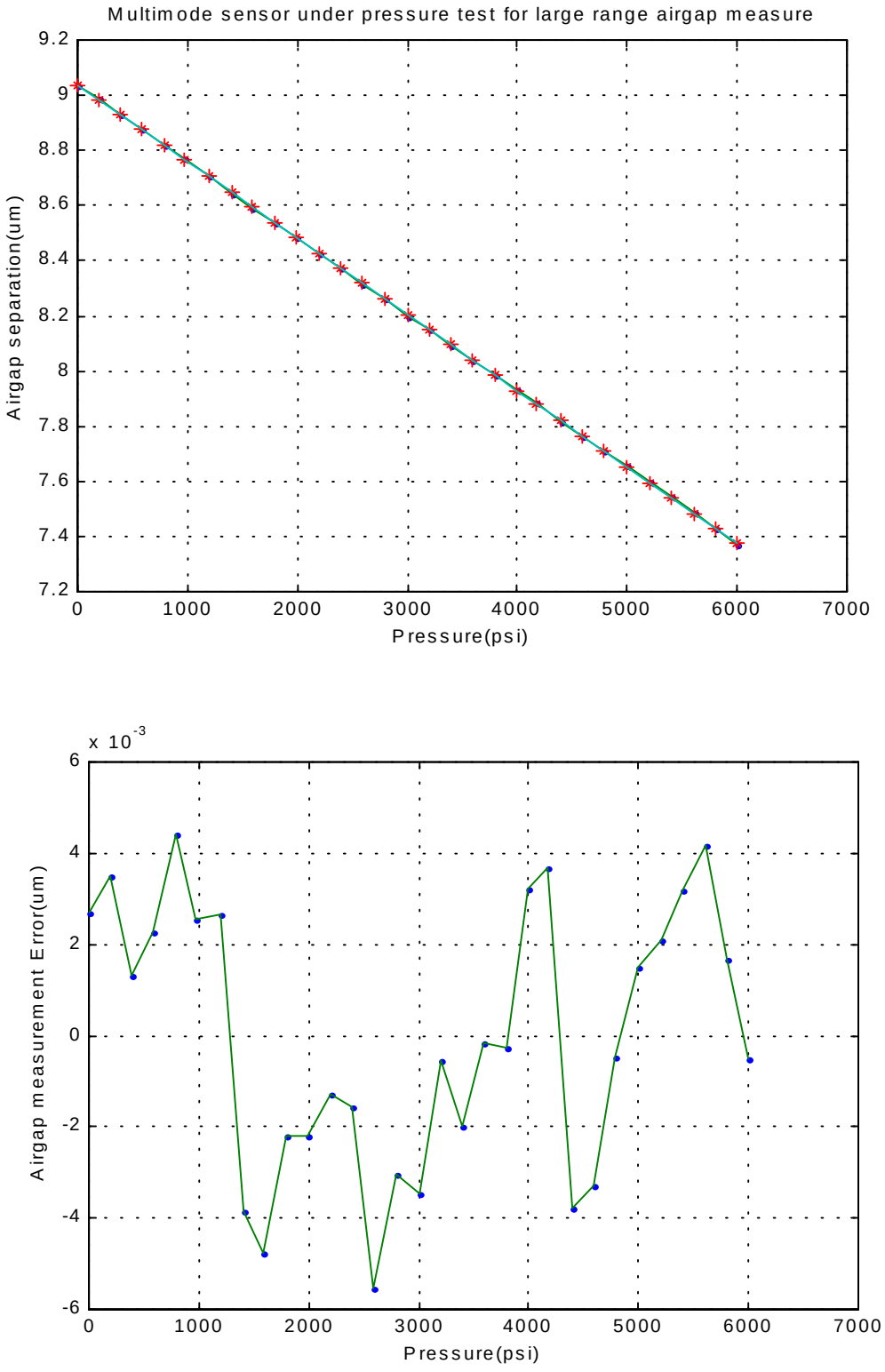

Figure 4.5. Air gap measurement performance in large dynamic range.

4.2 CO_2 Laser Power and Exposure Time Optimization

Thermal bonding is the most important step in sensor fabrication. When the tube and fibers assembly is exposed to CO_2 laser light, the optical energy is converted to heat energy which results in the increase of the temperature at the exposure area. If the temperature reaches the softening point of the silica glass material (about 1500°C), the tube and the fiber start to flow and join together. After the cooling, a solid bond is formed at the CO_2 laser exposure area. In order to achieve the best optical and mechanical performance of the fabricated sensor, the CO_2 laser exposure time and the power level need to be set to their optimal values. There are a few points that must be considered in choosing the exposure time and the power level.

First, to avoid excess residual stress from building in the bonding area, the increase and the decrease of the temperature should not be too fast. This results in an optimal design of the temperature increasing and the decreasing slope. Second, the glass materials should not be over-heated; otherwise the gravity will bend the fiber, which results in a large optical power loss at the bonding region. Therefore, the laser power needs to be set to an optimal level. Third, there is an optimal time duration in which the glass materials are soft and fluid. A review of fiber optic fusion splicer design reported in the technical literature suggests that the duration at which the glass is softened should be limited to a few seconds.

Based on the above considerations, we designed our CO_2 laser power and exposure time curve is shown in Figure 4.5. At first, we used 1 second of preheating time, 3 seconds of heating time with a laser power of 3watts and 1 second of annealing time. We found that after the laser was off, the tube was broken because of thermal shrinkage. After that, we increased the annealing time from 3 seconds to 10 seconds. The breakage problem was solved, and the sensor bonding looked tight. But when we put the sensor into liquid, it was leaking. This implied that the bonding was not complete. So we increased the laser power from 3watts to 4.7watts. At this time the backside of the tube was bonded with very good performance while the front side of the tube was over heated, which caused tube bending and larger optical loss. It is very difficult to transfer heat from one side to the other side uniformly.

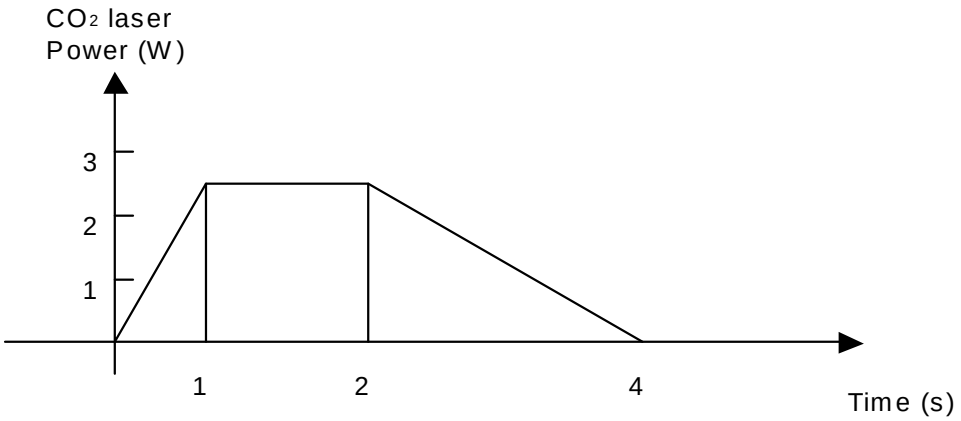

Figure 4.6 CO_2 laser power level and exposure time

One way to solve this problem is to use two CO_2 lasers simultaneously heating the sensor from different angles. But this method has three issues to be considered: 1) there is no room for another CO_2 laser around the sensor support system; 2) since CO_2 laser produces invisible light, it is very hard to align two laser beams on one line; 3) the cost is too high. In our system, we use two copper mirrors with 120^o angle to achieve energy uniform distribution. The spot shape of the CO_2 laser is rectangular. The size is 300 μm wide and 3500 μm long at the focus point. The focus distance of the cylindrical lens of CO_2 laser is 7.5 inch, so the tube was placed around the focus point. The diameter of the tube we used is 362 μm. From the geometry relationship, we get the distance between tube and the mirror in the range of 365 μm ~1650 μm. When using mirrors, the CO_2 laser power and pulse duration can be decreased greatly. The bonding performances without mirrors and with mirrors are shown in Figure 4.7 and Figure 4.8 respectively. We used a microscope to monitor the process of bonding. In Figure 4.8 (a), the upper tube is the image of the tube that shows the backside bonding. The lower tube is the real tube that shows the front side bonding of the tube. Both of them were used with the same CO_2 laser power and pulse duration parameters. Through a large number of experiments, we obtained a set of optimal parameters. We used CO_2 laser with 1 second of preheating time, 1 second with 2.3watts of heating time and 2 seconds of annealing time. From the experiments, we found that the single mode fiber sensor bonding is easier than the multimode fiber sensor bonding since single mode fiber sensor has less sensitivity to fiber misalignment than multimode fiber

sensor. So when fabricating the single mode sensor, CO_2 laser power and pulse duration parameters can be more flexible. For example, we can use the CO_2 laser with 1 second of preheating time, 0.6 to 1 second with 2.1 to 2.3watts of heating time and 2 seconds of annealing time. The total fabrication time is about 4 seconds.

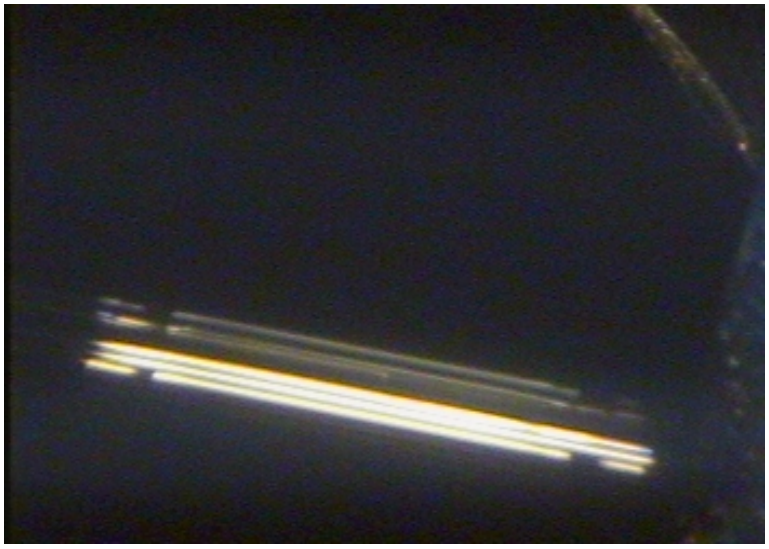

(a) Back side of the tube after bonding without mirrors.

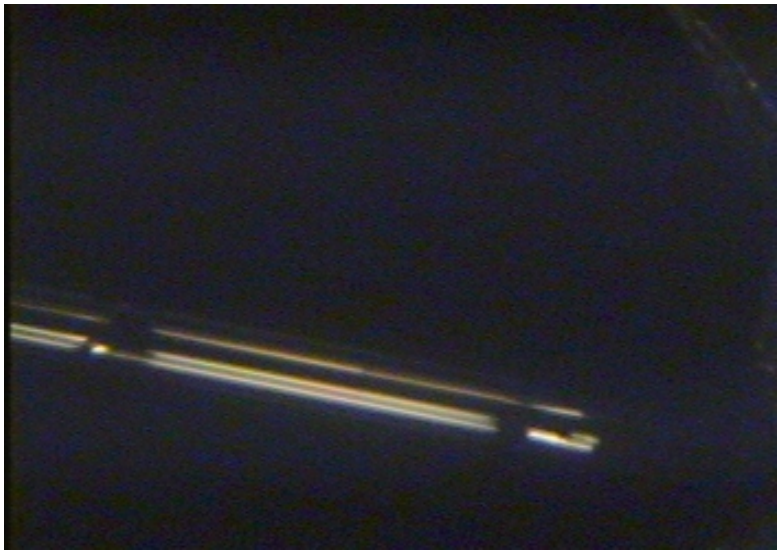

(b) Front side of the tube after bonding without mirrors.

Figure 4.7. Bonding without mirrors.

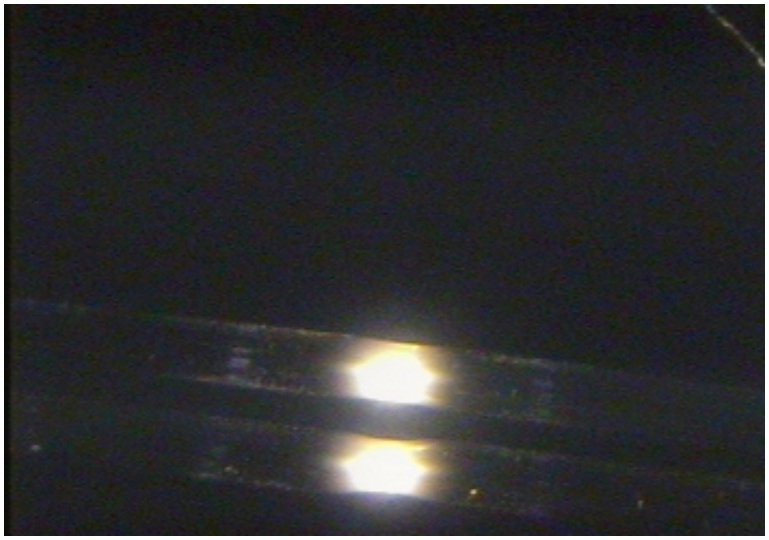

(a) Performance with mirrors when bonding.

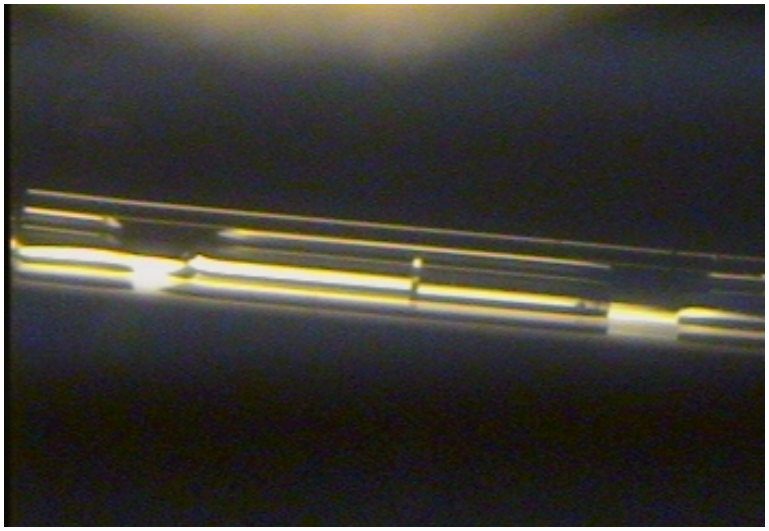

(a) Back side of the tube after bonding.

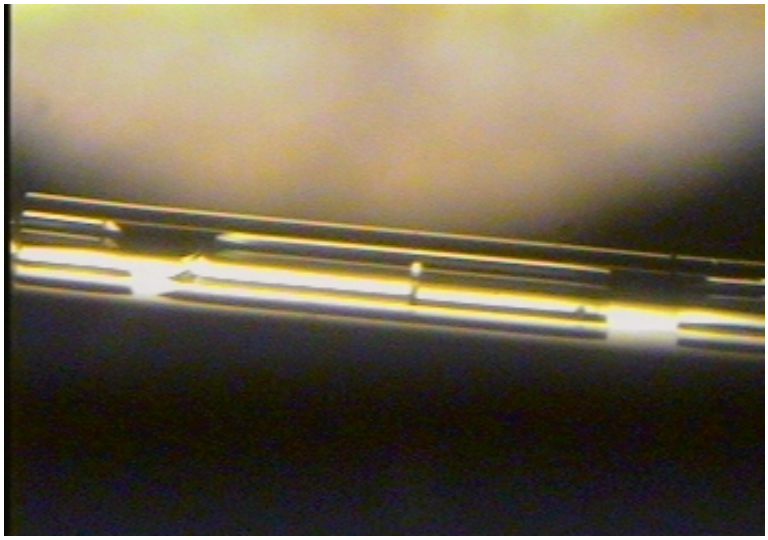

(c) Front side of the tube after bonding.

Figure 4.8. Bonding with mirrors.

4.3 PZT Stage Calibration

The final fine adjustment of the sensor air gap is achieved by moving the PZT stage. The movement of the PZT stage is controlled by the computer programs through a 16-bit D/A circuit and a PZT driver as illustrated in Figure 2.11. However, the relationship between the PZT displacement and the external control voltage is not linear. In order to adjust the air gap to a preset value at an ultra-high accuracy, we need to calibrate the PZT stage movement with respect to the input control voltage. The calibration was conducted by using the white light interferometer and an extrinsic Fabry-Perot interferometric (EFPI) sensor. First we implement an EFPI micro-displacement multimode sensor with one fiber sealed to the tube, and the other fiber fixed to the PZT stage. When the PZT stage moves, it generates an interferometric displacement signal through the EFPI sensor. At the same time, this interferometric signal is measured by the white light interferometric air gap monitoring system. Relating the PZT control voltage to the white light interferometer output, the PZT stage can be precisely calibrated. Figure 4.9 shows the PZT calibration results. The upper curve corresponds to the forward movement of the PZT, the lower curve corresponds to the backward movement of the PZT. By using the curve-fitting method, we can control the PZT stage movement with a very high accuracy by referring to the stored calibration data.

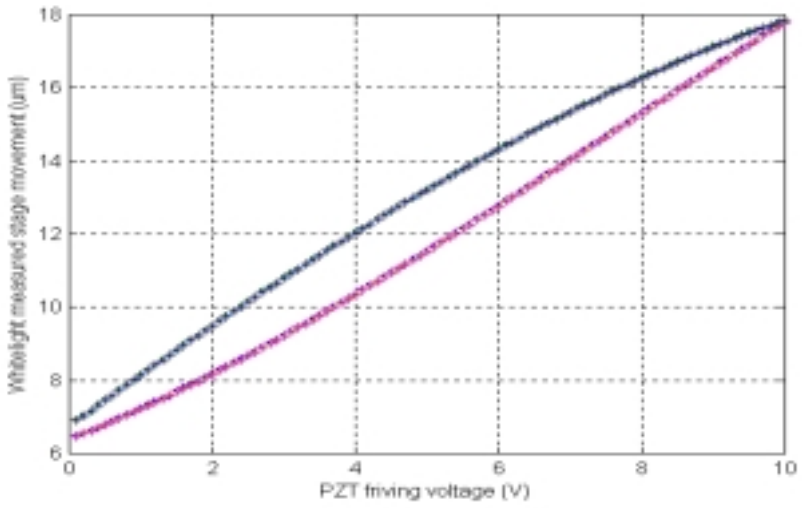

Figure 4.9. PZT stage movement calibration results.

4.4 Sensor Fabrication Experimentation

After many experiments and tests, we finalized all the parameters involved in the sensor fabrication. The final setup positions the tube and fiber assembly 10mm away from the CO_2 laser focal point. For multimode fiber tube based sensors, the full laser power is 2.3 watts, and for single mode fiber tube based sensors the full laser power is from 2.1 watts to 2.3 watts. The sensor bonding region has a typical size of 300 μm. The sensor gauge length can be chosen from 0.5 mm to 5 mm. The initial gap can be adjusted to any value with an accuracy of 0.02 μm. The bounding points have been tested to show good strength from the pressure test, and the sensor fabrication has a very good repeatability.

Many single mode and multimode fiber sensors have been fabricated to be used in temperature and pressure experiments. We represent the fabrication process and performance of temperature and pressure sensors in the following two sections.

4.4.1 SCIIB Temperature Sensor Fabrication and Testing Results

Novel SCIIB (Self-Calibrated Interferometric/Intensity Based) fiber optic sensor technology has been developed by the Photonics Laboratory at Virginia Tech [31]. The sensing scheme combines the advantages of both fiber interferometry sensors and intensity-based sensors.

The goal in the SCIIB temperature sensor is to precisely measure the temperature between –40ºC and +200ºC with accuracy of ±1.0ºC and resolution of 0.01ºC.

The SCIIB temperature sensor is fabricated through the sensor fabrication control system. The fabrication process involves inserting two cleaved fibers inside a capillary tube and using the CO_2 laser to thermally fuse the fibers and the tube together. The SCIIB temperature sensor fabrication requires precise control of the initial air gap so that the sensor has an initial operating point at the starting point of the linear portion of an interference fringe. The sensor effective gauge length can also be controlled during the fabrication by using a translation stage to move the bonding point with respect to the CO_2 laser beam. After the sensor is fabricated, another CO_2 laser exposure is applied to provide proper annealing to the bonding region so that the residual stresses can be significantly reduced. An important issue for investigation is the robustness and stability of the SCIIB temperature sensor under harsh conditions such as high temperature. To answer this question, we conducted an experiment to test the sensor survivability under high temperature. The experiment setup includes an electrical furnace which has a maximum temperature up to 1100°C, with an Omega CN76000 thermometer to read the temperature at an accuracy of 0.1°C. The SCIIB fiber optic sensor and the thermometer were arranged side by side in the oven, and the temperature was increased from room temperature to 900°C in a step of 10°C. Both the SCIIB sensor output and the thermometer output were recorded for comparison. The temperature sensor under test had an effective gauge length of 1 mm, and the initial air gap of 5.93 μm. The temperature sensor was tested in the furnace several times. The test results are plotted in Figure 4.10. As we see, the sensor successfully survived the test and the output was quite repeatable. The testing results also indicate that the sensor has a very good thermal stability.

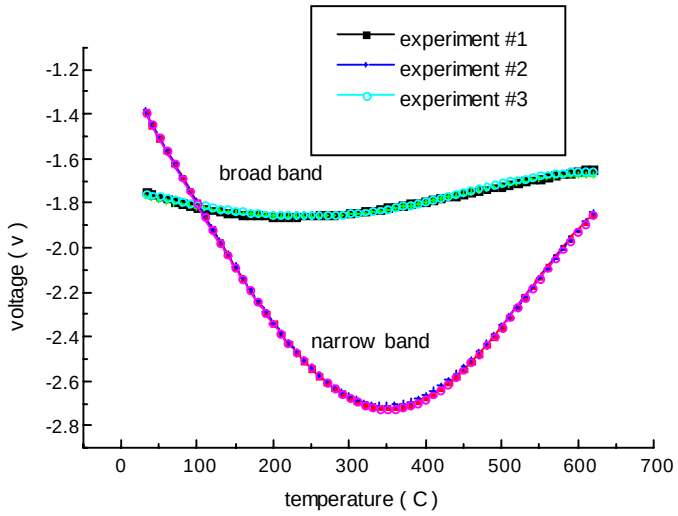

Figure 4.10. Temperature sensor survivability and stability test results.

4.4.2 Pressure Sensor Fabrication and Testing Results

Many pressure sensors were fabricated with the sensor fabrication control system. There are two important requirements that must be satisfied during the pressure sensor fabrication. First, the initial sensor air gap needs to be adjusted to the starting point of the linear portion of an interference fringe so that the operating region of the sensor covers the whole linear range of the sensor output. Second, the effective gauge length of the sensor should be adjusted to allow the fabrication of pressure sensors with different dynamic ranges.

The pressure sensor was tested with the APP pressure sensor calibrator. By increasing the pressure from the lower end to the higher end in steps, we recorded the SCIIB output at each step and curve fit those measured points to obtain a calibration curve. Figure 4.11 and Figure 4.12 illustrate the results of a multimode fiber pressure sensor for a pressure range of 1900psi. Figure 4.11 shows the linear range of this multimode fiber pressure sensor is from 0psi to 1900psi. Figure 4.12 shows the multimode fiber pressure sensor still has a very good reparability after an over pressure of 6000psi applied. Figure 4.13 shows the response of a

single mode fiber pressure sensor which has a linear range from 6000psi to 11000psi. Figure 4.14 shows the repeatability of the single mode fiber pressure sensor.

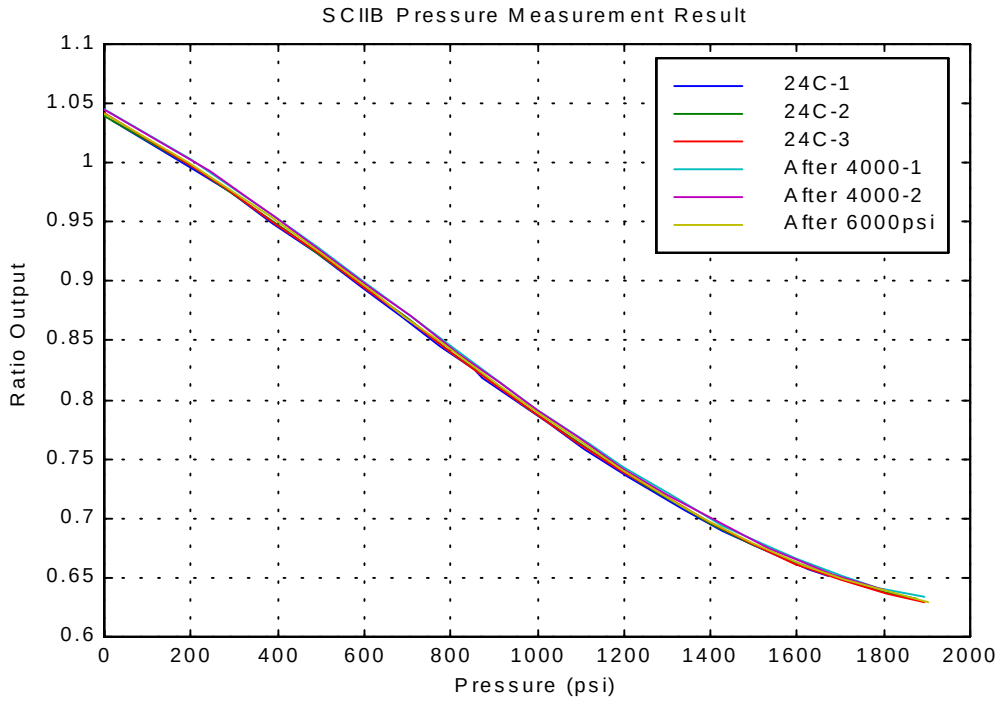

Figure 4.11. Linear pressure range for the multimode fiber sensor.

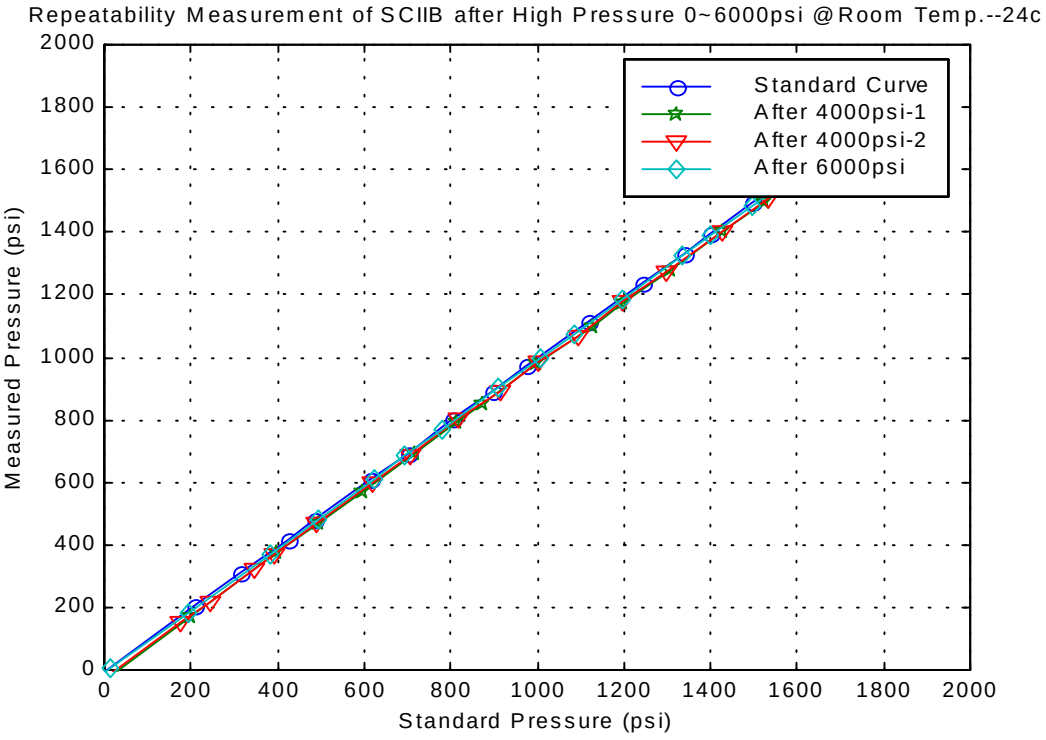

Figure 4.12. Repeatability of the multimode fiber sensor.

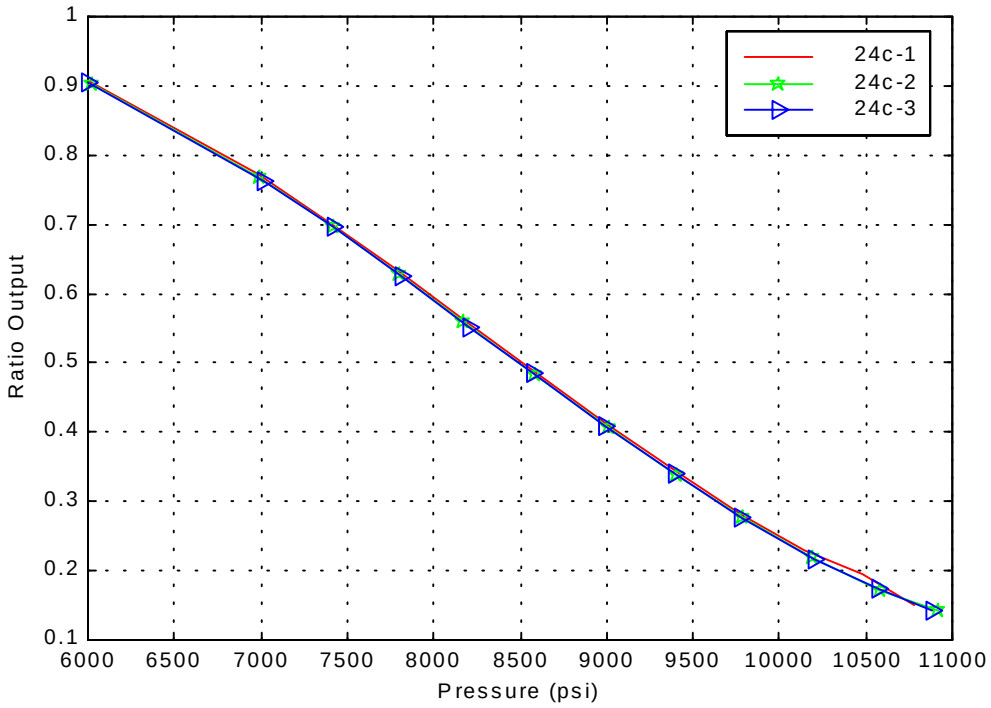

Figure 4.13. Linear range of the single mode fiber pressure sensor.

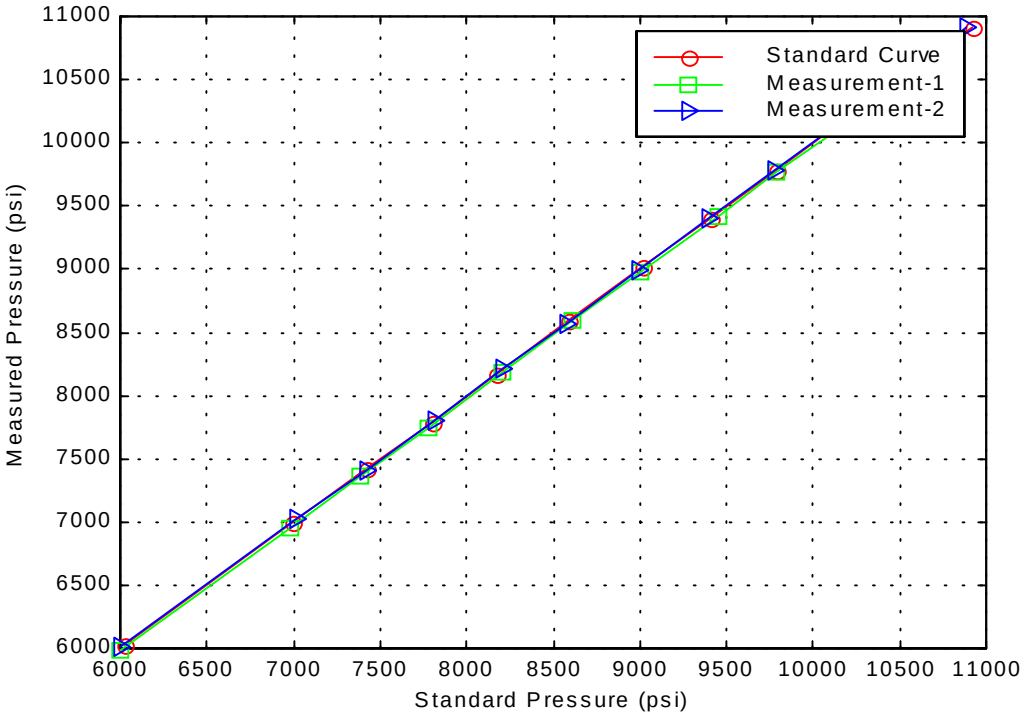

Figure 4.14. Repeatability of the single mode fiber sensor.

4.5 Error Analysis for Air Gap Separation Measurement

Many factors which can affect the accuracy of the air gap separation measurement, including software error and system error. In software, we normalized the spectrum to a sinusoidal curve, and employed FFT to dynamically determine the calculation window size, curve fitting to filter the noise, the mass central method to find peak and valley position, and one point tracing method to measure the air gap. These can maximally improve the accuracy and resolution of the air gap measurement. In the system, there are some factors which can cause an error of the air gap measurement. We will analyze each of them in the following sections.

4.5.1 Source Spectrum Change

The spectrum of an LED may change as ambient conditions vary. The spectrum change could be center wavelength shifts and/or spectral width widening. So we need to analyze the air gap measurement error caused by the shift and widening of the LED spectrum. From Equations (2-1) and (2-2), we define normalized signal S(k) to be the ratio of the signal returned from the sensor to the reference signal R(k) proportional to the original source spectral density distribution. They can be expressed as

$$R(k) = I_0 e^{-\frac{(k-k_0)^2}{\Delta k^2}} \qquad (4\text{-}1)$$

let $$k = 2\pi / \lambda \ ; \qquad (4\text{-}2)$$

$$S(k) = \frac{I_0 e^{-\frac{(k-(k_0+\delta_1))^2}{(\Delta k+\delta_2)^2}} \bullet (a + \cos(2kL))}{R(k)} \qquad (4\text{-}3)$$

Where L is the air gap separation (here we assume L = 8 μm);

λ is the central wavelength 850 nm;

$\Delta\lambda$ is the half spectral width (we choose $\Delta\lambda = \lambda_2 - \lambda_1$ = 880 nm- 820 nm = 60 nm);

k_0 corresponds to central wavelength λ_0;

$\Delta k = k_1 - k_2$, and $k_1 = 2\pi / \lambda_1$, $k_2 = 2\pi / \lambda_2$;

δ_1 is the shift of k_0;

δ_2 is the spectral width change;

Assuming there is $1nm$ center wavelength shift and $3nm$ width widening of LED spectrum, we use the mass central method to find peaks and valleys just like we did in the white light system program. Figure 4.15 plots the relationship between k and the intensity of the normalized signal. It demonstrates due to a left shift and a widening of the LED, the normalized spectrum is no longer symmetric. And the magnitudes of right side peaks are much higher than that of the left side. Figure 4.16 shows the air gap measurement error caused by the spectrum shifting and widening mentioned above.

Figure 4.16 also shows that the air gap measurement error by using adjacent valleys is less than that by using the peaks. In other words, valley measurement is more insensitive to the change of reference than peak measurement. So when we use one point tracing to accurately calculate the air gap, we trace valleys instead of peaks. In the case of only $1nm$ center wavelength shift of LED spectrum, the air gap measurement error is much smaller, which is within 0.4 nm. But with both $1nm$ center wavelength shift and $3nm$ width widening of LED spectrum, the air gap measurement error is 20nm by tracing one valley.

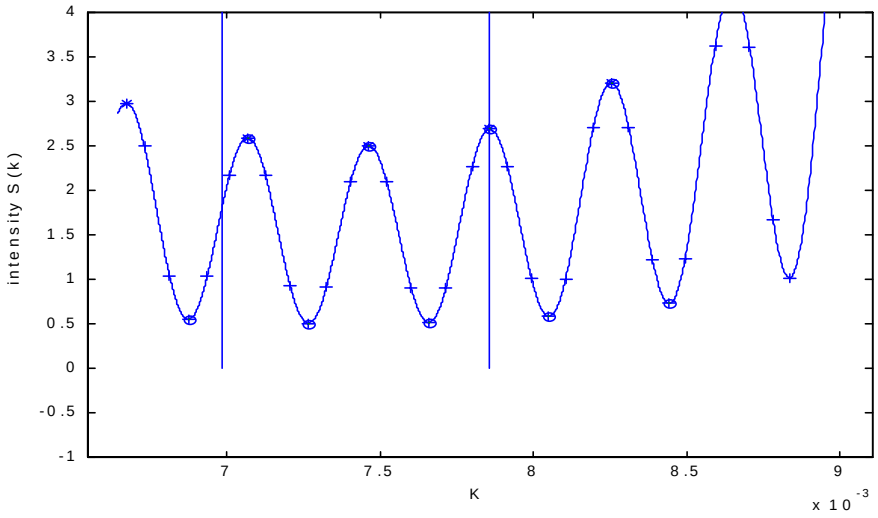

Figure 4.15. Relationship between k and intensity of the normalized signal.

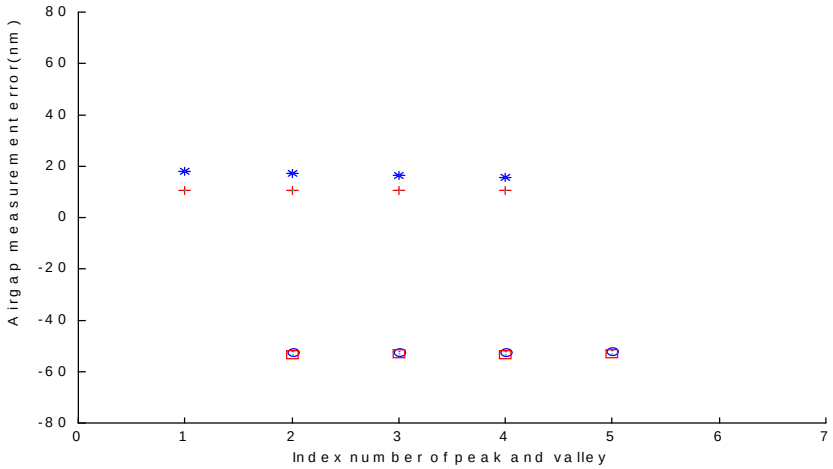

Figure 4.16. Air gap measurement error for each peak and valley.

'*' represents air gap measurement error when calculated in our theory with two adjacent valleys;

'+' represents air gap measurement error when using the mass central method with two adjacent valleys;

'o' represents air gap measurement error when calculated in theory with two adjacent peaks;

'⌂' represents air gap measurement error when using the mass central method with two adjacent peaks.

4.5.2 Banding Effect

Since bending fiber will change the distribution of modes in fibers, we bent the fiber, connected to the spectrometer, with diameters of 3/16, 5/32, and 1/8 inches to test fiber bending effects on the air gap measurement. The results show that there is 50 nm ~ 80 nm air gap measurement error caused by the bending. In our system, we reduced this effect by pre-bending the fiber.

4.5.3 Nonlinear Curve Fitting of the Spectrometer Card

As mentioned in Chapter 2, our system uses an Ocean Optics PC-2000 spectrometer card to process signal acquisition. The acquired data is an array of 2048 elements which correspond to 2048 pixel numbers. Each pixel number has a fixed relationship with a wavelength. This pixel-wavelength curve is calibrated and given by Ocean Optics Ins. We analyze here the

effects caused by nonlinear curve fitting and the error between the curve and the experiment points which are used to calibrate the curve.

First, we use the mass central method to find peaks and valleys.

Let: $$k = 1/\lambda \qquad (4\text{-}4)$$

We then have: $$K = \frac{\sum y_i k_i}{\sum y_i} \qquad (4\text{-}5)$$

y_i corresponds to the intensity of each wavelength. Considering the non-uniform intervals caused by the nonlinear curve fitting, which is shown in Figure 4.17, we modified Equation (4-5) as following:

$$K = \frac{\sum y_i (k_i - k_{i-1}) k_i}{\sum y_i (k_i - k_{i-1})} \qquad (4\text{-}6)$$

Second, the 3-order curve is calibrated through 12 experiment points. In Figure 4.18, we can see within the range from 800 nm to 900 nm, the curve fitting error will cause a wavelength error about 0.1 nm. According to Section 4.6.1, the corresponding air gap measurement error is about 1.5 nm. In order to reduce this effect, assuming the experimental points are accurate enough, we recalibrated the fitting curve from 800 nm to 900 nm since we only process data of this range to calculate air gap separations.

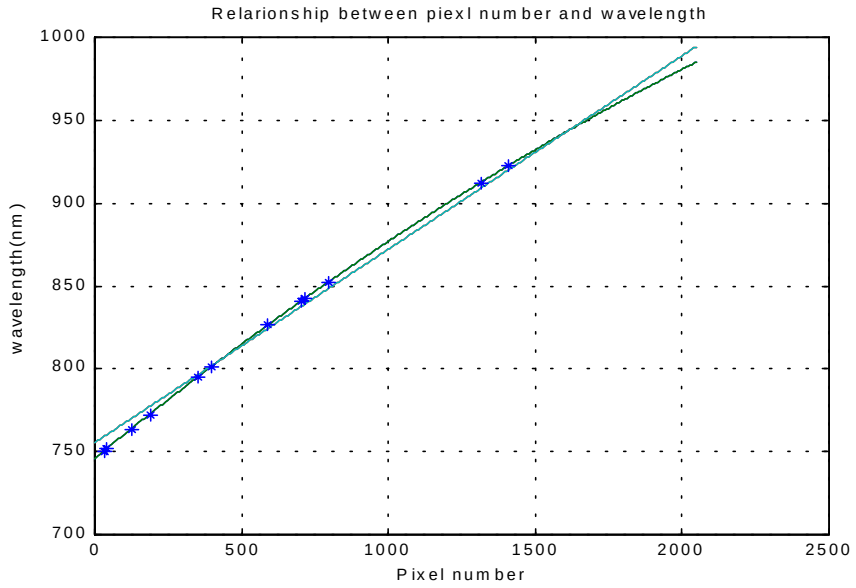

Figure 4.17. Relationship between pixel number and wavelength.

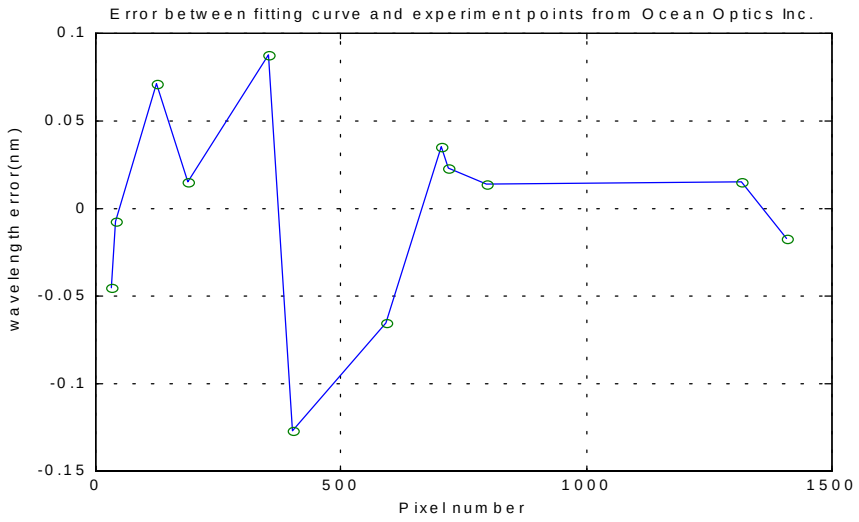

Figure 4.18. Wavelength error caused by curve fitting.

4.5.4 Tracing Different Peaks or Valleys

For an optimal system, tracing different points should yield the same result. Due to the system error described above, tracing different points will give different air gaps. We made a multimode sensor with L=9.591μm which had two peaks and two valleys in the range of 800 nm to 900 nm. After the temperature testing, we analyzed the following four cases:

1) Using adjacent peaks to measure air gap which is shown in Figure 4.19.

In Figure 4.19, we can see there is a "jump" during the air gap measurement. This is caused by the factors discussed in Section 2.2.2.

2) Using adjacent valleys to measure air gap which is shown in Figure 4.20.

In Figure 2.20, we can see that the "jump" problem is eliminated a lot, but the curve is still not linear. The improvement of air gap measurement compared to Figure 4.19 results because the wavelength measurement error by tracing valleys is more insensitive than that by tracing peaks.

3) Tracing one valley that is the nearest to the central wavelength to measure air gap which is shown in Figure 4.21. In Figure 4.21, we get a good linear curve of air gap change. This air gap measurement method is used in our sensor fabrication control system.

4) Tracing different valleys to measure air gap which is shown in Figure 4.22.

When the valley we are tracing moves out of the truncated window, the program need to find the next valley to trace. Figure 4.22 illustrate the air gap measurement error caused by tracing next valley. We can see the air gap measurement error is only ±2 nm.

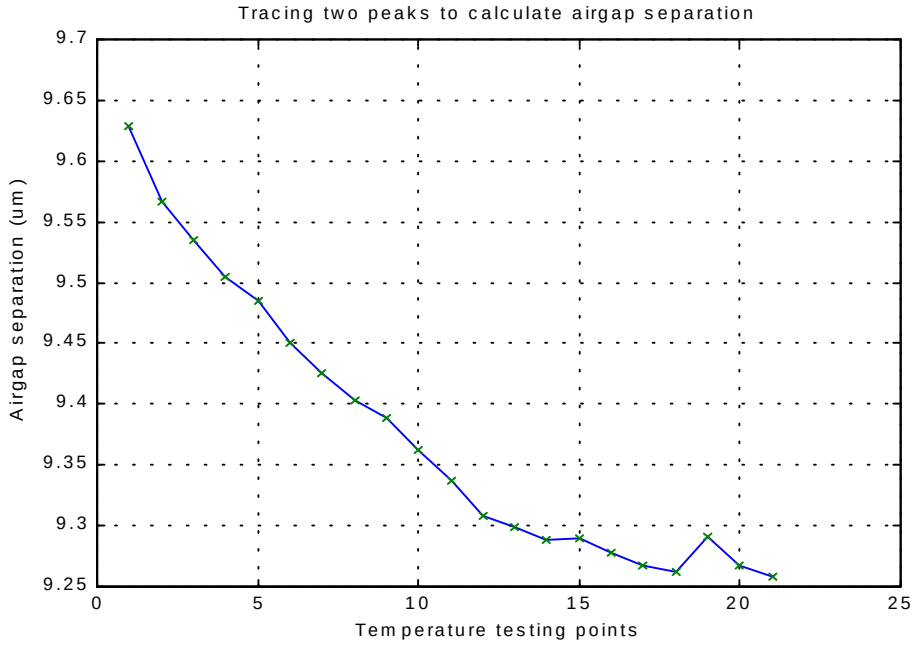

Figure 4.19. Air gap measurement performance by tracing two adjacent peaks.

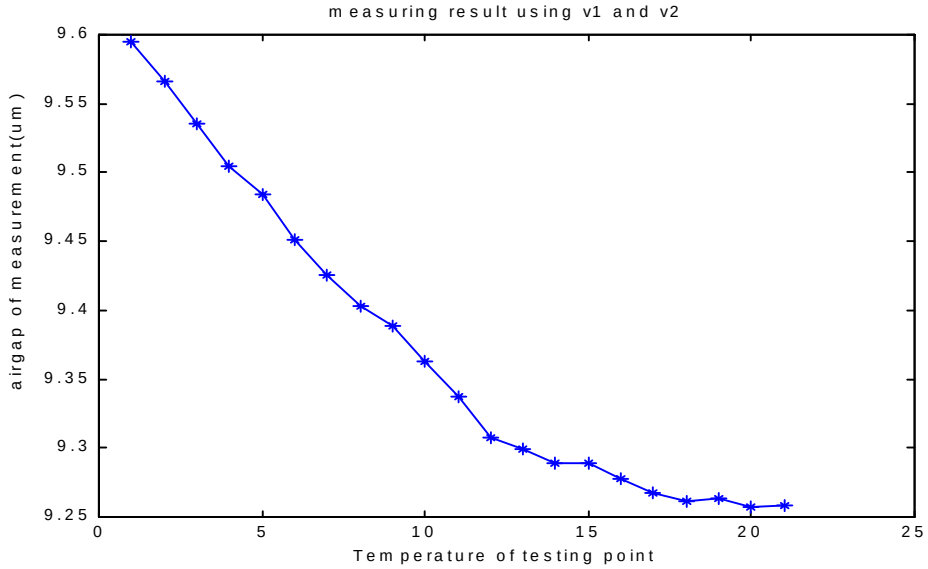

Figure 4.20. Air gap measurement performance by tracing two adjacent valleys.

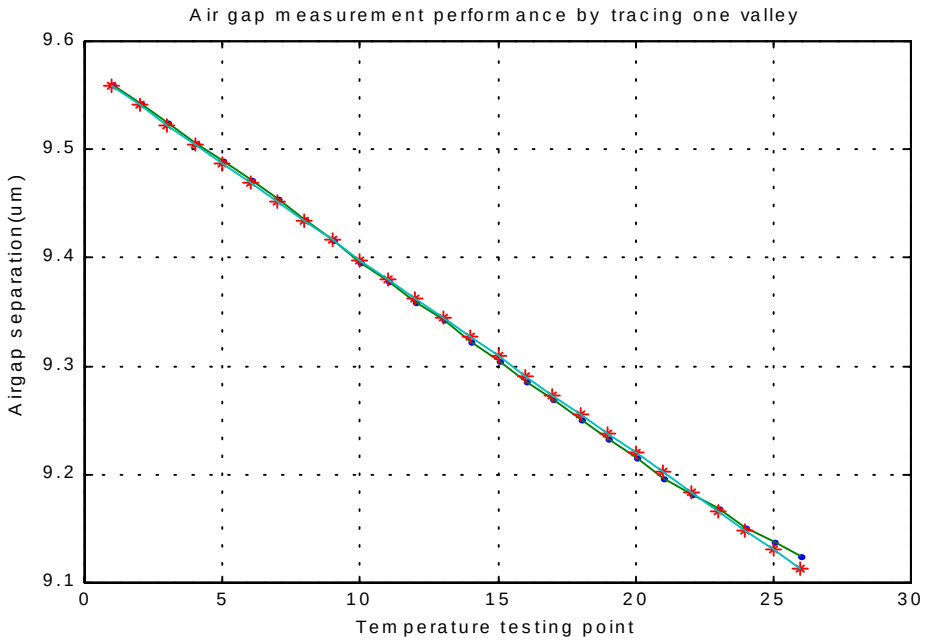

Figure 4.21. Air gap measurement performance by tracing one valley.

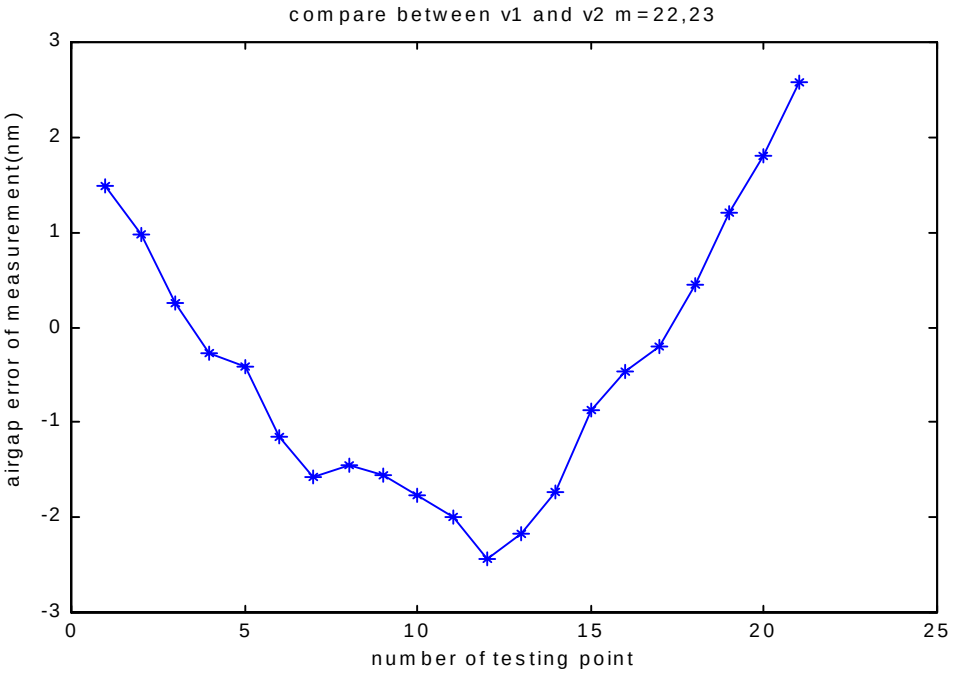

Figure 4.22. Air gap measurement error caused by tracing different valleys.

Chapter 5. Conclusion

A new system for controlled fabrication of EFPI sensors has been developed. The sensor fabrication control system includes a CO_2 laser subsystem as the heating source, a white light interferometric subsystem to monitor and control in real-time of the air gap separation in the EFPI sensor, and a X-Y translation stage/PZT micro-motion control subsystem for the sensor alignment as well as the air gap adjustment. A set of computer software with a graphical user interface (GUI) is designed for loop-control of the three subsystems. A large number of temperature and pressure sensors were fabricated by the use of this system, and the experimental testing of these sensors has proven the sensors to have excellent performance. During the sensors fabrication, the repeatability and reliability of the system have also been proven.

Using CO_2 laser to thermal bonding sensor is a novel technique. It overcomes the temperature and time dependability when using epoxy to bond the sensors.

The white light interferometric provides an absolute measurement with ultra-high accuracy and resolution of air gap separation in Fabry-Perot sensors. Unlike only tracing adjacent peaks, we combine absolute and relative measurement methods to improve the air gap measurement.

This research and resultant results have placed a solid foundation for achieving the long-term goal of automated sensor fabrication.

References

[1] E. Udd, “Fiber Optic Sensors An Introduction for Engineers and Scientists,” *John Wiley & Sons Inc.*, p 217,p 148,1991.

[2] R. J. Schroeder, R. T. Ramos, T. Yamate, “Fiber Optic Sensors for Oil Field Services,” *SPIE Proceedings*, Vol.3860, pp. 12.

[3] D. R. Huston, P. L. Fuhr, E. Udd, D. Inaudi, “Fiber Optic Sensors for Evaluation and Monitoring of Civil Structures,” *SPIE Proceedings*, Vol.3860, pp. 2.

[4] P. L. Fuhr, D. R. Huston, W. B. Spillman, “Multiplexed Fiber Optic Pressure and Vibration Sensors for Hydroelectric Dam Monitoring,” *SPIE Proceedings*, Vol.1798, pp. 247.

[5] Peter L. Fuhr, “The Development, Installation and Initial Results of Fiber Optic Chloride Sensors Embedded into Bridge Decks,” *SPIE Proceedings*, Vol.3538, pp. 311.

[6] Gang He, “A Fiber-Optic Medical Pressure-Sensoring System Employing Intelligent Self-Calibration,” *SPIE Proceedings*, Vol.2594, pp. 218.

[7] S. Quist, V. Martinelli and R. Ikeda, “Fiber-Optic Gyroscopes in Automotive and industrial Applications”, *Sensors*, Vol. 13, No. 4, pp. 42-46, April 1996.

[8] P. L. Fuhr and D. R. Huston, “Fiber Optic Smart Civil Structures”, *SPIE Proceedings*, Vol.2574, pp. 6-11, May 1995.

[9] S. Chen, A. W. Palmer, K. T. V. Grattan, and B. T. Meggit, “Digital signal-processing techniques for electronically scanned optical-fiber white-light interferometry,” *Applied Optics*, vol. 31, pp. 6003-6010, Oct. 1992.

[10] A Wang, S. Gollapudi, K. A. Murphy, R. G. May, R. O. Claus, “Sapphire-fiber-based intrinsic Fabry-Perot interferometeric sensors,” *Optics Letters*, v. 17, n. 14, 1992.

[11] A Wang, S. Gollapudi, R. G. May, K. A. Murphy, R. O. Claus, “ Advances in Sapphire-fiber-based interferometeric sensors,” *Optics Letters*, v. 17, n. 21, 1991.

[12] K. A. Murphy, M. S. Miller, A. M. Vengsarkar, R. O. Claus, “Elliptical-core, two-mode, optical fiber sensor implementation methods,” *J. Lightwave Tech.*, v. 8, n. 11, 1990.

[13] R. O. Claus, M. F. Gunther, A. Wang, and K. A. Murphy, “Extrinsic Fabry-Perot sensor for strain and crack opening displacement measurements from -200 to 900C,” *Smar Materials and Structures*, vol. 1, pp. 237-242, 1992.

[14] J. A. Greene, K. A. Murphy, B. R. Fogg, R. O. Claus, A. M. Vengsarkar, "Optical fiber, vibration mode filters incorporating photoinduced refractive index gratings," *Smart Materials and Structures*, v. 1, 1992.

[15] H. Xiao, W. Zhao, R. Lockhart, J. Wang, and A. Wang, Absolute sapphire optical fiber sensor for high-temperature applications, *SPIE-Int. Soc. Opt. Eng. Proc. of Spie — the Int. Soc. for Opt. Eng.* 3201 pp. 36-42, 1997.

[16] H. Xiao, Y. Xie, J. Deng, R. G. May, and A. Wang "Absolute Sapphire Optical Fiber Interferometric Sensors," *SPIE Proceedings*, Vol.3538, pp. 115, 1998.

[17] Vivek Arya, Marten J. de Vries, Madhu Athreya, Anbo Wang, Richard O. Claus, "Analysis of the effect of imperfect fiber endfaces on the performance of extrinsic Fabry-Perot interferometric optical fiber sensors"

[18] Al-Chalabi, S. A. Culshaw, B. and Davies, D. E. N., "Partially Coherent Sources in Interferometery," IEE No. 221 *Proceedings 1st International Conference on Optical Fiber Sensors*, London, pp 132, 1983.

[19] Bosselman, Th. and Ulrich, R., "High Accuracy position-sensing with fiber coupled white light Interferometers," IEE No. 221 *Proceedings 2nd International Conference on Optical Fiber Sensors*, Stuttgart, pp 361, 1984.

[20] K. T. V. Grattan, B. T. Meggitt, "Optical; Fiber Sensor Technology," *Chapman & Hall*, UK, pp269, 1995.

[21] Ocean Optics, Inc. "OOIWinIP Windows Interface Package Programmer's Guide", Version 3.00, February 1999.

[22] Anbo Wang, Mark S. Miller, David Sun, K. A. Murphy, and Richard O. Claus, "Advances in the extrinsic Fabry-Perot interferometric optical fiber sensors," *SPIE Proceedings*, Vol. 1798, pp. 32,1992.

[23] Chern-Lin Chen, Shun-Chung Wang, "A PC-Based Adaptive Software for Automatic Calibration of Power Transducers, " *IEEE Transactions on Instrumentation and Measurement*, Vol. 46, No. 5, October 1997.

[24] Dennis Kafura, "Object-oriented software design and construction with C++," *Prentice-Hall, Inc., Upper Saddle River, New Jersey*, 1998.

[25] Synrad, Inc. "Series 48 Lasers Operation and Service Manual", Release v4.0, September 1997.

[26] Tran, T. A., Greene, J. A., Jones, M.E. Grace, J., Murphy, K. A., and Claus, R. O., "Optical Fiber Sensor-Based Smart Materials and Structures," *Final Report for DARPA Grant* No. DAAH01-94-C-R010, 1995.
[27] Tran, T. A., "Digital Spectral Analysis and Adaptive Processing Techniques for Phase Modulated Optical Fiber Sensors," *Department of Electrical Engineering, Virginia Polytechnic Institute and State University*.
[28] Q. Wang, Y. N. Ning, K. T. V. Grattan, A. W. Palmer, "Signal processing scheme for central position identification in a white-light interferometric system with a dual wavelength source, " *Optics & Laser Technology*, Vol. 29, No. 7, pp. 377-382, 1997.
[29] "Instruction Handbook for the MELLES GRIOT Piezo Controllers 17 PCW 001(011) and 17 PCW 002(012)," Melles Griot, Cambridge, England.
[30] H. Xiao, W. Huo, J. Dend, M. Luo, Z. Wang, R. May, and A. Wang, "Fiber Optic Whitelight Interferometric Spectrum Signal Processing for Absolute Measurements," *Processing of SPIE*, vol. 3852, 19 Sept. 1999.
[31] G. Z. Wang, A. Wang, R. G. May, and R. O. Claus, "Self-referenced fiber optic sensor for microdisplacement measurement," *Optical Engineering*, vol. 34, pp. 240-243, Jan.1995.

Appendix

```
'-----------------------------------------------------------
'----    Copyright (c) 1999                          ----
'----    Photonics Labolatory                        ----
'----    EE Dept. Virgina Tech.                      ----
'----    Blacksburg, VA 24061                        ----
'-----------------------------------------------------------
Option Explicit

Global sp As SCANPARM                   ' Scan parameter structure
Global spv As SETPARMVAL                ' save current parameter values
Global offset As Double                 ' Wavelength offset
Global Coeff1 As Double                 ' First wavelength coefficient
Global Coeff2 As Double                 ' Second wavelength coefficient

Global DarkDat(2048) As Double          ' Dark scan values
Global RefDat(2048)  As Double          ' Reference scan values
Global SampDat(2048) As Double          ' Sample scan values
Global cDat(2048) As Double             ' calculate values cdat(i)=sampdat(i)/refdat(i)
Global Wavelen(2048) As Double          ' save wavelength as x axis values
Global BoxDat(2048) As Double
Global Ave_dark As Double               ‘ average dark to be used to decide start point and ending point

'---- save current parameter values ----
Type SETPARMVAL
        fdc As Integer              ' flash delay in msec
        dsf As Integer              ' sampling frequency (kHz - S1000, msec - S2000)
        boxcar As Integer           ' boxcar smoothing width
        average As Integer          ' samples to average
        chan_ena(3) As Integer      ' spectrometer channel enabled array
        scan_dark As Integer        ' scan dark
        correct_dark As Integer     ' correct for electrical dark signal
        extrig As Integer           ' external trigger mode
        Intercept As Double
        Coeff1 As Double
        Coeff2 As Double
End Type

Global Repeat As Integer            ' Repeating scan flag
Global PaintMode As Integer         ' Display mode
Global PlotMode As Integer          ' Decide whether plot or not.
                                    ' if plot, PlotMode=PLOT,else PlotMode=NoPLOT.
Global yscale As Double             ' detemined by view. scope is 10 and transmission is 1.
Global Window As Integer            ' used to find peak&Valey
Global Airgap_desired As Double
Global Airgap As Double
Global Num_p As Integer             ' the number of Peaks in find_Peaks function.
Global Num_v As Integer             ' the number of Valeys in find_Peaks function.
Global start_Point As Integer       ' starting point Pixel number of truncated window.
Global end_Point As Integer         ' end point Pixel number of truncated window.
Global startwv As Double            ' the start wavelength correspond to start_Point.
Global endwv As Double              ' the end wavelength correspond to end_Point.
```

```
'---the parameters bellow are for plot---'
Global Const PLOT = 1                ' if plot
Global Const NoPLOT = 0              ' if not plot
Global Const Scope = 0               ' Scope display
Global Const ABSORBANCE = 1              ' Absorbance display
Global Const TRANSMISSION = 2            ' Transmission display
Global X_org As Double
Global Y_org As Double
Global X_scale As Double                  ' local scale of x axis value
Global Y_scale As Double                  ' local scale of y axis value
Global max_peak, min_valey, visibility As Double
'---the parameters bellow are for saving file---'
Global Reffile As String
Global Trafile As String
Global Smpfile As String
'---the parameters bellow are for system---'
Global FiberMode As Integer              ' 1 for multimode system and 2 for singlemode system.
Global Record As Integer                 ' used for record airgap data in traceV-Gap function.
Global Response As Integer
Global trace_Flag As Boolean             ' determined in traceV-Gap function, and used for control
                                         ' the change of trac_Num.
Global trace_Num As Double               ' determined in traceV-Gap function.
Global report_PV As Integer              ' determined in traceV-Gap function, and reported in
                                         ' continue scan.
Global ValeyID(20) As Integer            ' determined in find_Peaks function, and used in
                                         ‘ traceV-Gap function.
Global PeakID(20) As Integer             ' stoer peaks & Valleys index number.
Function GetScan(Dcmd, flash) As Integer
'-----------------------------------------------------
'Dcmd value:
'       CMD_NONE = 0     no specific command
'       CMD_SETUP = 1    force hardware setup
'       CMD_STATUS = 2   send status message
'       CMD_TEST = 9     return test data
'
'flash value:
'       flash = 0       sp.scan_dark = 0
'       flash = 1       sp.scan_dark = 1
'-----------------------------------------------------
   Dim i As Integer
   sp.cmd = Dcmd                         ' Driver command
   sp.scan_dark = flash                  ' Flash control
   i = OOI_DoScan(sp)                    ' Execute a scan
   If i <> 0 Then                        ' if OOI_DoScan returns an error
     MsgBox ("OOI_DoScan returned " + Str(i)) ' display error
   End If
   Select Case (i)
      Case ER_TIMEOUT                    ' scan timed out
         MsgBox "Scan timed out"
      Case ER_BUSY                       ' hardware unavailable
         MsgBox "Hardware busy"
      Case ER_MEMORY                     ' insufficient memory free
         MsgBox "Insufficient memory"
      Case ER_UNKNOWN                    ' unknown instance (shouldn't happen)
         MsgBox "Process ID Unknown"
      Case ER_TIMER                      ' timer unavailable
```

```
        MsgBox "Timer unavailable"
      Case ER_ERROR                    ' other error
        MsgBox "Unknown error"
   End Select
   GetScan = i                         ' set return value
End Function


Public Function MassCenter_peak(StartIndex As Integer, StopIndex As Integer) As Double
'-------------------------------------------------------------------------------------------------------------------'
' Function:      Using mass central method to precisely find peak position.
' Input value:   StartIndex/StopIndex are the starting/ending point of the cutting part,
'                which are determined according to cutting level of the peak.
' Return value:  Wavelength of the peak.

' Note:          The equation of mass center is: x' = sum(x(i)*y(i)) / sum(y(i)).
'                x(i) is wavelength. y(i) is light intensity. x' is peak or Valey wavelen
'                we let f(i) = 1/x(i).  so the equation above is modified as:
'                f' = sum(f(i)*y(i)) / sum(y(i)). So x'=1/f'
'-------------------------------------------------------------------------------------------------------------------'
  Dim i As Integer, k As Integer, j As Integer
  Dim Max_array As Integer, n As Integer
  Dim x() As Double, y() As Double
  Dim Sfy As Double, sy As Double, Min As Double

  Sfy = 0: sy = 0
  Max_array = StopIndex - StartIndex + 1
  If Max_array <= 1 Then
     MsgBox "Airgap calculation is out of range in MassCenter_peak 1!"
     PaintMode = Scope
     MainForm.mnuScope.Checked = True          ' Mark scope menu item
     MainForm.mnuTransmission.Checked = False  ' Clear transmission menu item
     Exit Function
  Else
     ReDim x(Max_array)
     ReDim y(Max_array)
  End If
  k = 0
  '--find mininum value in the range from startindex to stopindex--'
  Min = 10000  ' initial a very big value
  For i = StartIndex To StopIndex
    If cDat(i) < Min Then Min = cDat(i)
  Next i
  For i = StartIndex To StopIndex
    x(k) = 1000 / Wavelen(i)
    y(k) = (cDat(i) - Min) * (1000 / Wavelen(i - 1) - 1000 / Wavelen(i))
    k = k + 1
  Next i
  For i = 0 To k - 1
    Sfy = Sfy + x(i) * y(i)
    sy = sy + y(i)
  Next i
  If Sfy = 0 Then
     MsgBox "Airgap calculation is out of range in MassCenter_peak 2!"
     PaintMode = Scope
     MainForm.mnuScope.Checked = True          ' Mark scope menu item
```

```
        MainForm.mnuTransmission.Checked = False    ' Clear transmission menu item
        Exit Function
    Else
        MassCenter_peak = sy * 1000 / Sfy                'feed back the peak wavelen
    End If
End Function
Public Function MassCenter_valey(StartIndex As Integer, StopIndex As Integer) As Double
'-------------------------------------------------------------------------------------------------------------'
' Function:       Using mass central method to precisely find valley position.
' Input value:    StartIndex/StopIndex are the starting/ending point of the cutting part,
'                 which are determined according to cutting level of the valley.
' Return value:   Wavelength of the valley.
' Note:           The equation of mass center is: x' = sum(x(i)*y(i)) / sum(y(i)).
'                 x(i) is wavelength. y(i) is light intensity. x' is peak or Valey wavelen.
'                 we let f(i) = 1/x(i).  so the equation above is modified as:
'                 f' = sum(f(i)*y(i)) / sum(y(i)). So x'=1/f'
'-------------------------------------------------------------------------------------------------------------'
    Dim i As Integer, k As Integer, j As Integer
    Dim Max_array As Integer, n As Integer
    Dim x() As Double, y() As Double
    Dim Sfy As Double, sy As Double, Min, max As Double

    Sfy = 0: sy = 0
    Max_array = StopIndex - StartIndex + 1
    If Max_array <= 1 Then
        MsgBox "Airgap calculation is out of range in MassCenter_valey 1!"
        PaintMode = Scope
        MainForm.mnuScope.Checked = True            ' Mark scope menu item
        MainForm.mnuTransmission.Checked = False    ' Clear transmission menu item
        Exit Function
    Else
        ReDim x(Max_array)
        ReDim y(Max_array)
    End If
    k = 0

    '--find maximum value in the range from startindex to stopindex--'
    max = 0                                         ' initial a very big value
    For i = StartIndex To StopIndex
      If cDat(i) > max Then max = cDat(i)
    Next i
    For i = StartIndex To StopIndex
      x(k) = 1000 / Wavelen(i)
      y(k) = (max - cDat(i)) * (1000 / Wavelen(i - 1) - 1000 / Wavelen(i))
      k = k + 1
    Next i
    For i = 0 To k - 1
      Sfy = Sfy + x(i) * y(i)
      sy = sy + y(i)
    Next i
    If Sfy = 0 Then
        MsgBox "Airgap calculation is out of range in MassCenter_valey 2!"
        PaintMode = Scope
        MainForm.mnuScope.Checked = True            ' Mark scope menu item
        MainForm.mnuTransmission.Checked = False    ' Clear transmission menu item
        Exit Function
```

```
  Else
     MassCenter_valey = sy * 1000 / Sfy                  'feed back the peak wavelen
  End If
End Function
'-- this function is for drawing the axises when need plotting --'
Public Function Draw_axis() As Integer
   MainForm.Cls
   MainForm.ForeColor = QBColor(0)
   '-- X range is from 740-1050nm --'
   MainForm.Line (X_org, Y_org)-((X_org + 310 * X_scale), Y_org)
   '-- Y range is from 0-4100 in scope mode or 0-410 in transmission mode --'
   MainForm.Line (X_org, Y_org)-(X_org, (Y_org - 4200 * Y_scale))
   MainForm.Line (1470, 1035)-(1530, 1035)
   MainForm.Line (1470, 2367.5)-(1530, 2367.5)
   MainForm.Line (2700, 3670)-(2700, 3730)
   MainForm.Line (3700, 3670)-(3700, 3730)
   MainForm.Line (4700, 3670)-(4700, 3730)
   MainForm.Line (5700, 3670)-(5700, 3730)
   MainForm.Line (6700, 3670)-(6700, 3730)
End Function
'-- this function is to form Boxdat(2048) from sp.sdat(i) --'
Public Function Scan_dat() As Integer
   Dim Response As Integer, i As Integer, k As Integer
   Dim ss As Double, temp(2048) As Double

   Response = GetScan(CMD_NONE, 0)
   For i = 0 To 2047
      SampDat(i) = sp.sdat(i, 0)                    ' Save sample data as pixel number
   Next i
   ' minuse DarkDat(i) from sample data to form temp(i) '
    For i = 0 To 2047
      If (SampDat(i) - DarkDat(i)) <= 1 Then
         temp(i) = 1
      Else
         temp(i) = SampDat(i) - DarkDat(i)
      End If
    Next i
    ' use spv.boxcar to curve the sample, form boxdat(i) '
    If spv.boxcar > 0 Then
      For k = 0 To spv.boxcar - 1
         BoxDat(k) = temp(k)
      Next k
      For k = spv.boxcar To (2047 - spv.boxcar)
         ss = 0
         For i = 0 To 2 * spv.boxcar
            ss = ss + temp(k - spv.boxcar + i)
         Next i
         BoxDat(k) = ss / (1 + 2 * spv.boxcar)
      Next k
      For k = (2047 - spv.boxcar + 1) To 2047
         BoxDat(k) = temp(k)
      Next k
   Else
      For k = 0 To 2047
         BoxDat(k) = temp(k)
      Next k
```

```
    End If
End Function


Public Function traceV_gap(point1 As Integer, point2 As Integer) As Double
'*************************************************************************'
' Function:        Trace Valley which is nearest to central wavelength to calculate
'                   airgap.
' Input value:     point1/point2 is the starting/ending point of the truncate window,
'                  which are determined according to avg_dark.
' Return value:    airgap.
' only use mass central method to find peak and valley
' Modified on April 11th, 2000 as following:
' 1)only using valley-valley value to calculate caorse airgap;
' 2)recalibrate the curve just from 800nm to 900nm; change the coefficients
' 3)fixed the calculation range from 800nm to 900nm; the corresponding pixel
'   numbers are start_point=750 and end_point=1590.
' 4)separate peaks and valleys into two arrays. simplify the program.--May, 29th.
'*************************************************************************'
    Dim i As Integer
    Dim j As Integer
    Dim k As Integer
    Dim MinDat As Double
    Dim MaxDat As Double
    Dim p_Edge As Double
    Dim v_Edge As Double
    Dim point As Integer
    Dim peakwv(20) As Double
    Dim valeywv(20) As Double

    Dim p_StartPoint As Integer  ' peak starting index in mass central
    Dim p_EndPoint As Integer    ' peak ending index in mass central
    Dim v_StartPoint As Integer  ' valley starting index in mass central
    Dim v_EndPoint As Integer    ' valley ending index in mass central


    'used for tracing single valley to calculate airgap
    Dim wave_pre As Double
    Dim wave_rel As Double
    Dim V_fix As Double
    Dim trace_Num1 As Double
    Dim p1 As Integer
    Dim p2 As Integer
    Dim pv_Num As Integer
    Dim valid_P As Integer
    Dim valid_V As Integer
    Dim coarse_Gap As Double
    Dim Win_Local As Integer
    ' Initialization
    For i = 0 To 19
        peakwv(i) = 0
        valeywv(i) = 0
    Next i
    Num_p = 0
    Num_v = 0
    p1 = p2 = 0
```

```
v_Edge = 0
p_Edge = 0
report_PV = 0

'-------------------------------------------------------------------------------------------------'
' form ID() and return number of p&v
pv_Num = Find_Peaks(point1, point2)
If pv_Num < 2 Then
   MainForm.promotion.Text = "out of range:too small Airgap"
   MainForm.tbairgap.Text = ""
   PaintMode = Scope
   MainForm.mnuScope.Checked = True          ' Mark scope menu item
   MainForm.mnuTransmission.Checked = False  ' Clear transmission menu item
   Exit Function
End If

'when pv_Num >= 2, that is at least one peak and one valley after coarse finding pv

' -------------for each peak------------------
valid_P = 0
For i = 0 To Num_p - 1
   ' 1. find cutting level for each peak
   If ValeyID(i) <> 0 Then
      p_Edge = cDat(PeakID(i)) - (cDat(PeakID(i)) - cDat(ValeyID(i))) * 0.3
      Win_Local = Abs(PeakID(i) - ValeyID(i)) * 0.7
   Else
      p_Edge = cDat(PeakID(i)) - (cDat(PeakID(i)) - cDat(ValeyID(i - 1))) * 0.3
      Win_Local = Abs(PeakID(i) - ValeyID(i - 1)) * 0.7
   End If

   ' 2. find starting and ending range for determining start and end points for peak
   If PeakID(i) - Win_Local < point1 Then
      p1 = point1
   Else
      p1 = PeakID(i) - Win_Local
   End If
   If PeakID(i) + Win_Local > point2 Then
      p2 = point2
   Else
      p2 = PeakID(i) + Win_Local
   End If

   ' 3. find starting and ending points for peak
   p_StartPoint = 0
   p_EndPoint = 0
   For point = p1 To p2
      If cDat(point) < p_Edge And cDat(point + 1) > p_Edge Then
         p_StartPoint = point
      End If

      If cDat(point) > p_Edge And cDat(point + 1) < p_Edge Then
         p_EndPoint = point
      End If
   Next point

   ' 4. determine the valid peak anf find fine peak wavelength
```

```
    If p_StartPoint <> 0 And p_EndPoint <> 0 Then
       peakwv(valid_P) = MassCenter_peak(p_StartPoint, p_EndPoint)
       valid_P = valid_P + 1
    End If
  Next i ' process next coarse peak

  ' -----------------for each valley------------------
  valid_V = 0
  For i = 0 To Num_v - 1
    ' 1. find cutting level for each valley
    If PeakID(i) <> 0 Then
       v_Edge = cDat(ValeyID(i)) + (cDat(PeakID(i)) - cDat(ValeyID(i))) * 0.3
       Win_Local = Abs(PeakID(i) - ValeyID(i)) * 0.7
    Else
       v_Edge = cDat(ValeyID(i)) + (cDat(PeakID(i)) - cDat(ValeyID(i - 1))) * 0.3
       Win_Local = Abs(PeakID(i) - ValeyID(i - 1)) * 0.7
    End If

    ' 2. find starting and ending range for determining start and end points for valley
    If ValeyID(i) - Win_Local < point1 Then
       p1 = point1
    Else
       p1 = ValeyID(i) - Win_Local
    End If
    If ValeyID(i) + Win_Local > point2 Then
       p2 = point2
    Else
       p2 = ValeyID(i) + Win_Local
    End If

    ' 3. find starting and ending points for valley
    v_StartPoint = 0
    p_EndPoint = 0
    For point = p1 To p2
       If cDat(point) > v_Edge And cDat(point + 1) < v_Edge Then
          v_StartPoint = point
       End If

       If cDat(point) < v_Edge And cDat(point + 1) > v_Edge Then
          v_EndPoint = point
       End If
    Next point

    ' 4. determine the valid valley anf find fine valley wavelength
    If v_StartPoint <> 0 And v_EndPoint <> 0 Then
       valeywv(valid_V) = MassCenter_valey(v_StartPoint, v_EndPoint)
       valid_V = valid_V + 1
    End If
  Next i ' process next coarse valley

  report_PV = valid_P + valid_V
  If report_PV < 2 Then
    MainForm.promotion.Text = "out of range:too small Airgap in traceV_gap 1"
    MainForm.tbairgap.Text = ""
    PaintMode = Scope
    MainForm.mnuScope.Checked = True          ' Mark scope menu item
```

```
        MainForm.mnuTransmission.Checked = False  ' Clear transmission menu item
        Exit Function
    End If

    ' calculate caorse airgap
    If report_PV = 2 Then
       traceV_gap = (0.25 * valeywv(0) * peakwv(0) / Abs(peakwv(0) - valeywv(0))) / 1000
    End If
    If valid_P = 2 And valid_V = 1 Then ' two peaks and one valley
       'using two peaks or two valleys to calculate airgap
        coarse_Gap = (0.5 * peakwv(0) * peakwv(1) / (peakwv(1) - peakwv(0))) / 1000
    Else
        ' have more than 2 valleys.
        'first using middle two valleys to calculate coarse airgap
        coarse_Gap = 0.5 * valeywv(Int(valid_V / 2) - 1) * valeywv(Int(valid_V / 2)) / (valeywv(Int(Num_v / 2)) -
valeywv(Int(valid_V / 2) - 1))
        coarse_Gap = coarse_Gap / 1000
    End If

    'only initialize once
    If (trace_Flag) Then
        'trace the valley position nearest to central wavelength
        V_fix = 0
        For i = 1 To valid_V - 1
            If Abs(valeywv(i) - 850) < Abs(valeywv(V_fix) - 850) Then
                V_fix = i
            End If
        Next i
        trace_Num = 2 * coarse_Gap * 1000 / valeywv(V_fix)
        trace_Flag = False
    End If
    'On Error GoTo PeakError

    ' find the real valley wavelength which we are tracing
    wave_pre = 2 * 1000 * coarse_Gap / trace_Num

    ' if the traced valley is moved out of the window, then recalculate the new trace_Num
    If (wave_pre > 870) Or (wave_pre < 830) Then ' for multimode 800/900
        V_fix = 0
        For i = 1 To valid_V - 1
            If Abs(valeywv(i) - 850) < Abs(valeywv(V_fix) - 850) Then
                V_fix = i
            End If
        Next i
        trace_Num1 = 2 * coarse_Gap * 1000 / valeywv(V_fix)
        trace_Num = trace_Num + Int(trace_Num1 - trace_Num + 0.5)
        wave_pre = 2 * 1000 * coarse_Gap / trace_Num
    End If

    ' find the real valley position which is the nearst to the wave_pre
    wave_rel = valeywv(0)
    For i = 1 To valid_V - 1
        If Abs(valeywv(i) - wave_pre) < Abs(wave_rel - wave_pre) Then
            wave_rel = valeywv(i)
        End If
    Next i
```

```
    ' accurate airgap can be got by tracing one valley
    If wave_rel <= 0 Then
        MsgBox "Airgap calculation is out of range in traceV_gap 2!"
        PaintMode = Scope
        MainForm.mnuScope.Checked = True          ' Mark scope menu item
        MainForm.mnuTransmission.Checked = False  ' Clear transmission menu item
        Exit Function
    Else
        trace_Num1 = 2 * coarse_Gap * 1000 / wave_rel
    End If
    trace_Num = trace_Num + Int(trace_Num1 - trace_Num + 0.5)
    traceV_gap = wave_rel * trace_Num / (2 * 1000)

    If Record = 1 Then
        Open "D:\DOE\mid_result\peak_valley.txt" For Append As #1
        Write #1, "peak wavelengths"
        For i = 0 To (valid_P - 1)
            Write #1, peakwv(i)
        Next i
        Write #1, "valley wavelengths"
        For i = 0 To (valid_V - 1)
            Write #1, valeywv(i)
        Next i
        Write #1,
        Close #1

        Open "D:\DOE\mid_result\traceNum.txt" For Append As #1
        Write #1, trace_Num, wave_pre, wave_rel
        Close #1
        Record = 0
    End If
'PeakError:
'   MsgBox "Airgap calculation is out of range!"
'   PaintMode = Scope
'   MainForm.mnuScope.Checked = True          ' Mark scope menu item
'   MainForm.mnuTransmission.Checked = False  ' Clear transmission menu item
'   Exit Function
End Function

Public Function Find_Peaks(point1 As Integer, point2 As Integer) As Double
'*************************************************************************************'
' Function:       Find coarse peaks & Valleys ID number to provide the distance of
'                 adjacent peak and valley for the determination of mass central
'                 cutting levels.
' Input value:    wv1/wv2 is the starting/ending point of the trauncut window,
'                 which are determined correspond to the range from 800nm to 900nm.
' Return value:   the number of peaks+valleys.
' Use moving window (31 for single mode, and 71 for multi mode) to find peak and
' valley positions.
'*************************************************************************************'
    Dim i As Integer
    Dim j As Integer
    Dim ValeyIndex As Integer
    Dim PeakIndex As Integer    ' the position of Valey
    Dim MinDat As Double
```

```
    Dim MaxDat As Double

    For i = 0 To 19
        ValeyID(i) = 0
        PeakID(i) = 0
    Next i
    Num_p = 0
    Num_v = 0
    '----------------- Find Peaks ID and Peak wavelengths ----------------------'
    For j = point1 To point2 - Window
        'find max value within the Window.
        MaxDat = 0
        For i = j To Window + j - 1
            If cDat(i) > MaxDat Then
                MaxDat = cDat(i)
                PeakIndex = i
            End If
        Next i
        ' check if this position is in the middle of the window.
        If (PeakIndex = j + (Window - 1) / 2) And (PeakIndex + Window - 1 <= point2) Then
            PeakID(Num_p) = PeakIndex
            Num_p = Num_p + 1
        End If
    Next j ' end of j

    '----- find Valey position and value -----
    For j = point1 To point2 - Window
        MinDat = 1000
        For i = j To Window + j - 1
            If cDat(i) < MinDat Then
                MinDat = cDat(i)
                ValeyIndex = i
            End If
        Next i
        If (ValeyIndex = j + (Window - 1) / 2) And (ValeyIndex + Window - 1 <= point2) Then
            ValeyID(Num_v) = ValeyIndex
            Num_v = Num_v + 1
        End If
    Next j
    ' return number of peaks and valleys
    Find_Peaks = Num_p + Num_v
    ' Calculate the fringe visibility
    If Num_p <> 0 And Num_v <> 0 Then
        MaxDat = 0
        MinDat = 0
        For i = 0 To Num_p - 1
            MaxDat = MaxDat + cDat(PeakID(i))
        Next i
        For i = 0 To Num_v - 1
            MinDat = MinDat + cDat(ValeyID(i))
        Next i
        MaxDat = MaxDat / Num_p
        MinDat = MinDat / Num_v
        visibility = (MaxDat - MinDat) / (MaxDat + MinDat)
    end If
End Function
```

Vita

Wei Huo was born in Dalian, Liaoning province, PR China on July 31, 1964. She graduated with a Master of Design Engineering from Dalian University of Technology, Dalian, China in December 1989, and a Bachelor of Design Engineering from Dalian University, Dalian, China in August 1986. From 1991 to 1997, she worked as senior structural design engineer at Dalian Residential Building Design Firm. She joined the Photonics Laboratory at Virginia Tech in January 1998 as a M.S. student. Her professional interests include fiber optic sensors, computer software development and networking communications.